IMA Journal of Numerical Analysis (2018) **00**, 1–32
doi:10.1093/imanum/dry078

Long-time $L^\infty(L^2)$ *a posteriori* error estimates for fully discrete parabolic problems

Oliver J. Sutton
School of Mathematical Sciences, University of Nottingham, University Park, Nottingham NG7 2RD, UK
Oliver.Sutton@nottingham.ac.uk

[Received on 22 February 2018; revised on 10 August 2018]

Computable estimates for the error of finite element discretisations of parabolic problems in the $L^\infty(0,T;L^2(\Omega))$ norm are developed, which exhibit constant effectivities (the ratio of the estimated error to the true error) with respect to the simulation time. These estimates, which are of optimal order, represent a significant advantage for long-time simulations and are derived using energy techniques based on elliptic reconstructions. The effectivities of previous optimal-order error estimates in this norm derived using energy techniques are shown numerically to grow in proportion to either the simulation duration or its square root, a key disadvantage compared with earlier estimators derived using parabolic duality arguments. The new estimates form a continuous family, almost all of which are new, reproducing certain familiar energy-based estimates well suited for short-time simulations and not available through the parabolic duality framework. For clarity, we demonstrate the technique applied to a linear parabolic problem discretised using standard conforming finite element methods in space coupled with backward Euler and Crank–Nicolson time discretisations, although it can be applied much more widely.

Keywords: finite element method; *a posteriori* error estimation; parabolic problems; backward Euler time stepping; Crank–Nicolson time stepping.

1. Introduction

An unavoidable fact of life when simulating physical phenomena is that the approximate solutions produced by discrete schemes, such as finite element methods and related methods, will not perfectly match the true solutions of the model, resulting in some discretisation error. A natural question this raises, and one into which a breathtaking quantity of work has been invested, is whether this discretisation error can be quantified for a given simulation, knowing only the problem data and computed approximate solution. Such *computable a posteriori error estimates* can then be used to determine how faithful the discrete solutions are to the model, thus providing an indication of the reliability of the simulation and opening the door to the development of rigorous adaptive algorithms. Although the derivation of such error estimates for models based on systems of elliptic partial differential equations is by now rather mature (we refer to Ainsworth & Oden, 2000; Brenner & Scott, 2008; Verfürth, 2013, for instance), interesting open questions still remain for models based on parabolic and hyperbolic partial differential equations.

For linear second-order parabolic problems, there are two particularly natural norms in which to measure the error, the $L^2(0,t;H^1(\Omega))$ norm and the $L^\infty(0,t;L^2(\Omega))$ norm (a description of the notation we use here for Sobolev spaces and their associated norms is given in Section 2; for further details on these and Bochner spaces see Adams & Fournier, 2003), both of which arise through

conventional energy arguments. Optimal-order *a posteriori* estimates for the error in the $L^2(0,t;H^1(\Omega))$ norm may be proven using direct energy arguments, as shown by Picasso (1998) and Chen & Feng (2004). Although the same arguments provide a bound for the (higher-order) error in the $L^\infty(0,t;L^2(\Omega))$ norm, the resulting estimators are in fact of suboptimal order. The literature also includes a variety of *a posteriori* error estimates in other norms, including estimates in higher-order norms such as those of $L^\infty(0,t;H^1(\Omega))$ and $H^1(0,t;L^2(\Omega))$ shown by Lakkis & Makridakis (2006), maximum norm estimates of Kopteva & Linss (2013, 2017), estimates in general $L^r(0,t;L^\rho(\Omega))$ and $L^r(0,t;W^{1,\rho}(\Omega))$ norms due to Verfürth (1998a,b) and estimates of the $L^2(0,t;H^1(\Omega))\cap H^1(0,t;H^{-1}(\Omega))$ norm of the error developed, for instance, by Verfürth (2003), Ern & Vohralík (2010), Ern *et al.* (2017) and Gaspoz *et al.* (2018).

Optimal-order estimates for the $L^\infty(0,t;L^2(\Omega))$ norm error were first proven by Eriksson & Johnson (1991, 1995) using duality techniques. A significant recent breakthrough, however, was the introduction of the *elliptic reconstruction* technique by Makridakis & Nochetto (2003), allowing optimal-order error estimates to be derived in the $L^\infty(0,t;L^2(\Omega))$ norm via energy arguments by introducing 'elliptic reconstructions' of the discrete solution. The role these reconstructions play in the derivation of the error estimates may be seen as an *a posteriori* counterpart to the role of the Ritz projection in the derivation of optimal-order *a priori* error estimates in the $L^\infty(0,t;L^2(\Omega))$ norm, first deployed by Wheeler (1973). This splits the error into an elliptic component, which is treated using *a posteriori* error estimates derived for an associated elliptic problem, and a parabolic component that satisfies a differential equation with data which may be controlled at optimal-order. In the fully (space and time) discrete setting, these *a posteriori* error bounds are typically proven by combining the elliptic reconstruction in space with a suitable piecewise polynomial time reconstruction. An overview of this methodology is given by Makridakis (2007), and the combination of space and time reconstructions has shown itself to be very flexible in many settings. For example, optimal order $L^\infty(0,t;L^2(\Omega))$ error estimates have been proven using this technique for standard conforming finite element methods, coupled with backward Euler (Lakkis & Makridakis, 2006), Crank–Nicolson (Bänsch *et al.*, 2012, 2013; Lozinski *et al.*, 2009), fractional θ-step (Karakatsani, 2012), two-step backward differentiation (Sen Gupta *et al.*, 2016) and general *hp* discontinuous Galerkin (Georgoulis *et al.*, 2017) time-stepping schemes, to name but a few.

A problem plaguing the above $L^\infty(0,t;L^2(\Omega))$ norm error estimates derived using energy techniques with elliptic reconstructions, however, is that their *effectivity*, the ratio of the estimated error to the true error (a measure of the quality of the estimate), grows with the simulation time. For reasons discussed below and demonstrated numerically in Section 5, this growth typically occurs at rate t or $\sqrt{t}$ for a simulation of length t. Since this growth is independent of the discretisation parameters it does not prevent the estimates being of asymptotically optimal-order, but it is less than desirable from the perspective of obtaining good estimates of the discretisation error, particularly for long-time simulations. It is interesting to note that this growth does not occur for the duality-based $L^\infty(0,t;L^2(\Omega))$ error estimates of Eriksson & Johnson (1991, 1995), and the cause of this problem can be directly attributed to the way in which the terms of the error estimate accumulate with time. The true error accumulates through time in an $L^\infty(0,t)$ fashion, which is mimicked by the duality-based estimates where the various estimator components also accumulate through time in an $L^\infty(0,t)$ manner. Estimators derived through energy arguments, however, typically involve terms measuring the various sources of discretisation error accumulating through time in $L^1(0,t)$ or $L^2(0,t)$ norms, leading to error estimators that grow rapidly even when the error itself may not. The inherent problem with such an estimate can be seen by considering the situation where equally large errors are committed on each time step of the simulation; in this case, an $L^1(0,t)$- or $L^2(0,t)$-type accumulation of the error will grow at rate t or $\sqrt{t}$, respectively,

while an $L^\infty(0,t)$-type accumulation will remain constant. It is this gap between rates of accumulation that manifests itself as ever-growing effectivities.

The main result of this paper, Theorem 4.11, addresses this shortcoming. New estimates are introduced for the error in the $L^\infty(0,t;L^2(\Omega))$ norm, in which the individual estimator terms are permitted to accumulate through time in $L^p(0,t)$ norms for any $p \in [1,\infty]$. The derivation of these estimates is based on energy techniques through elliptic reconstructions and, to the best of our knowledge, their structure is completely novel, providing a wide variety of different bounds simultaneously, almost all of which are new. In particular, this family includes the familiar elliptic reconstruction-based estimates built on $L^1(0,t)$- and $L^2(0,t)$-type accumulations, while also allowing counterparts to the duality-based estimators incorporating $L^\infty(0,t)$-type accumulations to be derived using energy techniques. The key advantage of this is that, since the estimator terms can therefore accumulate through time in the same norm as the error, they exhibit effectivities that in practice appear to remain bounded with respect to the simulation length, typically tending to some constant value. As such, these estimates are very well suited for long-time simulations.

The technique for deriving these error estimates is essentially due to the structure of the partial differential equation. The proof relies on an appropriate *error equation*—a partial differential equation satisfied by the error with 'data' terms that may be controlled computably. The terms arising from this error equation are then estimated in a spatial manner, resulting in an ordinary differential equation through time for the $L^2(\Omega)$ norm of the error. The novelty that we offer is in how the 'data' terms of this ordinary differential equation are accumulated through time to provide an estimate of the $L^\infty(0,t;L^2(\Omega))$ norm of the error. Ultimately, the technique mirrors a classical trick, well known from the *a priori* error analysis of discretisations of parabolic problems, of applying a Poincaré–Friedrichs inequality to remove the H^1 norm of the error from the left-hand side of the error equation, providing instead a bounded exponential factor on each term of the estimate. This is encapsulated in Lemma 4.10, cf. Thomée (2006, Chapter 1), which provides the analogous *a priori* argument. We note that an outwardly similar exponential factor appears in the final-time error bounds in the $L^2(\Omega)$ norm of Lakkis *et al.* (2015, Section 6) and the final-time $L^\infty(\Omega)$ norm bounds of Kopteva & Linss (2013, 2017). The difference is in how this exponential factor is used; here it allows us to apply a Hölder inequality over the time domain (see Lemma 4.9), producing an estimate with general $L^p(0,t)$-type accumulations, while in the aforementioned final-time bounds it provides a 'forgetfulness' property to the estimator that is broadly related to the smoothing properties of the differential operator.

The technique demonstrated here is applied to numerical schemes consisting of a conforming finite element discretisation in space coupled with either a backward Euler or Crank–Nicolson time-stepping scheme. To present the essence of the technique in its simplest form, we remove a considerable layer of notation and technicalities by primarily focussing on the case of a single fixed spatial mesh. A side effect of this simplification is that we are able to present a slightly simplified version of the quadratic time reconstruction used by Akrivis *et al.* (2006), Lozinski *et al.* (2009) and Bänsch *et al.* (2012, 2013) to derive optimal-order $L^\infty(0,t;L^2(\Omega))$ error estimates for the Crank–Nicolson scheme. We further refine the results of Bänsch *et al.* (2012, 2013) by deriving estimates in which the data approximation term is of optimal order even when the forcing term is nonzero on the boundary of the domain. This loss of optimality was due to the fact that the data approximation terms of the previous estimates involved the projection of the forcing data onto discrete functions that satisfy zero boundary values, which is suboptimal when the forcing function is nonzero on the boundary.

It should be stressed, however, that the assumption of a fixed spatial mesh is purely for presentational convenience and the new approach to time accumulation is independent of the spatial mesh, and whether it is fixed or variable. To exhibit this, in Section 4.6 we briefly recall the additional (spatial) contributions

to the error estimate measuring mesh modification in the framework of a finite element discretisation with backward Euler time stepping in which the meshes may vary between time steps (after Lakkis *et al.* (2015)), and show how in this case the approach to time accumulation behaves exactly as for the fixed mesh. For a deeper discussion of the effects of mesh modification in the context of an adaptive algorithm for very general polygonal meshes built on a spatial discretisation using a virtual element method (Beirão da Veiga *et al.*, 2013; Cangiani *et al.*, 2017; Sutton, 2017a) with backward Euler time stepping, which adopts the present technique for time accumulation, we refer the reader to Sutton (2017b).

We introduce the model parabolic problem in Section 2 and its discretisation in Section 3. The *a posteriori* error estimates are then derived in Section 4 and their practical performance is assessed through a set of numerical examples in Section 5. Finally, we present some conclusions in Section 6.

2. Model problem

Let $T > 0$, and let $\Omega \subset \mathbb{R}^d$ be a bounded open domain with $d = 2, 3$. For simplicity, we assume that the domain Ω is a convex polygon, although the results we present could be extended to nonconvex domains with reentrant corners through the careful application of weighted estimates; see, for example, Wihler (2007) and Liao & Nochetto (2003).

The model problem we consider is to find $u : [0, T] \times \Omega \to \mathbb{R}$ satisfying

$$\begin{aligned} u_t(t,x) - \mathcal{A}u(t,x) &= f(t,x) && \text{for } (t,x) \in (0,T] \times \Omega, \\ u(x,0) &= u_0(x) && \text{for } x \in \Omega, \\ u(t,x) &= 0 && \text{for } (t,x) \in (0,T] \times \partial\Omega. \end{aligned} \tag{2.1}$$

Here $\mathcal{A}$ is a self-adjoint positive definite second-order linear elliptic operator of the form

$$\mathcal{A}v = \nabla \cdot (A \nabla v) - \mu v, \tag{2.2}$$

where $\mu \in L^2(\Omega)$ with $\mu(x) \geqslant 0$ almost everywhere on Ω, and $A : \Omega \to \mathbb{R}^{d \times d}$ is symmetric and positive definite for almost every $x \in \Omega$. Let $a : H_0^1(\Omega) \times H_0^1(\Omega) \to \mathbb{R}$ denote the bilinear form

$$a(v,w) = (A\nabla v, \nabla w) + (\mu v, w), \tag{2.3}$$

where $(v,w) := \int_\Omega vw \, \mathrm{d}x$ denotes the $L^2(\Omega)$ inner product. Further, for $\omega \subset \mathbb{R}^m$ and an integer $m > 0$, we use $\|\cdot\|_{W^{k,p}(\omega)}$ and $|\cdot|_{W^{k,p}(\omega)}$ to denote the standard norm and seminorm on the Sobolev space $W^{k,p}(\omega)$ for $k > 0$ and $p \in [1, \infty]$ (for further details, see Adams & Fournier, 2003, for example). For the special case of $\omega = \Omega$ we shall denote the $L^2(\Omega)$ norm by $\|\cdot\|$ and the $H^k(\Omega)$ norm by $\|\cdot\|_k$.

We note that a induces a norm on $H_0^1(\Omega)$, which we denote by $a(v,v) = |||v|||^2$. We further observe that a is continuous in this norm, and under the assumptions above $|||\cdot|||$ is equivalent to the standard $H^1(\Omega)$ norm, i.e., there exists a constant $\gamma \in \mathbb{R}$ such that

$$\gamma^{-1} \|v\|_1 \leqslant |||v||| \leqslant \gamma \|v\|_1 \tag{2.4}$$

for all $v \in H_0^1(\Omega)$.

The problem can therefore be written in weak form: find $u \in L^2(0,T;H^1_0(\Omega))$ with partial (time) derivative $u_t \in L^2(0,T;H^{-1}(\Omega))$ such that

$$(u_t(t),v) + a(u(t),v) = (f(t),v) \quad \text{for all } v \in H^1_0(\Omega) \text{ and a.e. } t \in [0,T], \tag{2.5}$$

where we have used the same notation to denote the $L^2(\Omega)$ inner product and the $H^1(\Omega)$–$H^{-1}(\Omega)$ duality pairing. Standard arguments ensure that this problem posesses a unique solution; see Evans (2010).

3. Numerical discretisation

We now recall the ingredients of a conventional conforming finite element discretisation of (2.5) with backward Euler or Crank–Nicolson time stepping.

3.1 *Spatial discretisation*

Let $\mathscr{T}_h$ be a shape-regular partition of the domain $\Omega \subset \mathbb{R}^d$ into nonoverlapping elements that are either d-dimensional simplices or hypercubes. To avoid extra technicalities we suppose that the elements in the mesh are either all simplices or all hypercubes. We denote by Γ_h the *skeleton* of the mesh $\mathscr{T}_h$; for $\Omega \subset \mathbb{R}^2$ this is the collection of element edges, while for $\Omega \subset \mathbb{R}^3$ it is the collection of element faces. We further introduce the mesh dependent norms

$$\|\cdot\|_{\mathscr{T}_h} := \left(\sum_{K\in\mathscr{T}_h} \|\cdot\|^2_{L^2(K)}\right)^{1/2} \quad \text{and} \quad \|\cdot\|_{\Gamma_h} := \left(\sum_{s\in\Gamma_h} \|\cdot\|^2_{L^2(s)}\right)^{1/2}, \tag{3.1}$$

and the piecewise constant mesh-size function $h : \Omega \to \mathbb{R}$ such that $h|_K = \operatorname{diam}(K)$ for each $K \in \mathscr{T}_h$ and $h|_s = \operatorname{diam}(s)$ for each $s \in \Gamma_h$.

The conventional conforming finite element function spaces with respect to $\mathscr{T}_h$ are then given by

$$V_h = \left\{v \in H^1(\Omega) : v|_K \in V_h^K \quad \text{for all } K \in \mathscr{T}_h\right\} \quad \text{and} \quad V_{h0} = V_h \cap H^1_0(\Omega), \tag{3.2}$$

where

$$V_h^K := \begin{cases} \mathbb{P}_k^K & \text{if } K \text{ is a simplex,} \\ \mathbb{Q}_k^K & \text{if } K \text{ is a hypercube.} \end{cases} \tag{3.3}$$

Here $\mathbb{P}_k^K$ denotes the space of polynomials of total degree k on K, and $\mathbb{Q}_k^K$ denotes the space of tensor-product polynomials of maximum degree k on K.

The assumptions on the mesh and discrete space above ensure the existence of a *Clément-type interpolation operator*, satisfying the following approximation estimate.

LEMMA 3.1 (Clément-type interpolation estimate, cf. Clément, 1975). For any $v \in H^1_0(\Omega)$ there exists $v_I \in V_{h0}$ such that

$$|v_I|_{H^1(K)} \leqslant C_{\text{interp}} |v|_{H^1(\widehat{K})}, \tag{3.4}$$

$$\left\|h^{-1}(v - v_I)\right\|_K \leqslant C_{\text{interp}}|v|_{H^1(\widehat{K})}, \tag{3.5}$$

$$\left\|h^{-1/2}(v - v_I)\right\|_s \leqslant C_{\text{interp}}|v|_{H^1(\widehat{s})} \tag{3.6}$$

for all $K \in \mathscr{T}_h$ and $s \in \Gamma_h$, where C_{interp} is a positive constant depending only on the shape regularity of $\mathscr{T}_h$. Here $\widehat{K}$ and $\widehat{s}$ denote the usual *finite element patch* of K and s, respectively, defined as the union of all mesh elements with which they share a vertex.

We define the *discrete spatial operator* $\mathcal{A}_h : V_{h0} \to V_{h0}$ satisfying

$$\big(\mathcal{A}_h w_h, v_h\big) = -a\big(w_h, v_h\big) \quad \text{for all } v_h \in V_{h0}, \tag{3.7}$$

and the $L^2(\Omega)$-orthogonal projectors $\mathcal{P} : L^2(\Omega) \to V_h$ and $\mathcal{P}_0 : L^2(\Omega) \to V_{h0}$, which satisfy

$$\big(\mathcal{P}v - v, v_h\big) = 0 \quad \text{for all } v_h \in V_h \qquad \text{and} \qquad \big(\mathcal{P}_0 v - v, v_h\big) = 0 \quad \text{for all } v_h \in V_{h0}, \tag{3.8}$$

respectively. The key difference between these is that the latter imposes zero Dirichlet boundary data. Finally, for quantities that may be discontinuous across the mesh skeleton, we define the *jump operator* $[\![\cdot]\!]$ across a mesh interface $s \in \Gamma_h$ as

$$[\![\boldsymbol{v}]\!]|_s = \begin{cases} \boldsymbol{v}^+ \cdot \boldsymbol{n}_s^+ + \boldsymbol{v}^- \cdot \boldsymbol{n}_s^- & \text{if } s \cap \partial\Omega = \emptyset, \\ 0 & \text{otherwise.} \end{cases} \tag{3.9}$$

Here we have used the following notation: if $s \cap \partial\Omega = \emptyset$, then there exist K^+ and K^- such that $s \subset \partial K^+ \cap \partial K^-$; the trace of the vector-valued function $\boldsymbol{v}$ on s from within $K^\pm$ is therefore denoted by $\boldsymbol{v}^\pm$, and $\boldsymbol{n}_s^\pm$ denotes the unit outward normal on s with respect to $K^\pm$.

3.2 *Temporal discretisation*

Suppose $\{t^n\}_{n=0}^N$ forms a partition of $[0, T]$, and let $\tau_n = t^n - t^{n-1} > 0$ for $n \in \{1, \ldots, N\}$. For $n \in \{1, \ldots, N\}$, the *discrete time derivative* $\partial^n : V_h \to V_h$ is defined for a set of functions $\{w_h^n\}_{n=0}^N \subset V_h$ by

$$\partial^n w_h^n := \frac{w_h^n - w_h^{n-1}}{\tau_n}. \tag{3.10}$$

For the remainder of the article we shall suppress the superscript on this operator, denoting $\partial = \partial^n$.

3.3 *Discrete numerical schemes*

We now introduce the backward Euler and Crank–Nicolson schemes for computing discrete approximations to the solution of (2.5). With clear ambiguity, we shall refer to the solutions obtained at the time nodes t^n using either scheme as $\{U^n\}_{n=0}^N \subset V_{h0}$, since throughout it shall be clear from the context which we are referring to.

3.3.1 *Backward Euler time discretisation.* The backward Euler scheme for approximating solutions to (2.5) reads as follows: given $U^0 = Iu_0$ find the sequence of finite element functions $\{U^n\}_{n=1}^N \subset V_{h0}$ satisfying

$$\big(\partial U^n, v_h\big) + a\big(U^n, v_h\big) = \big(f^n, v_h\big) \quad \text{for all } v_h \in V_{h0} \text{ and } n \in \{1, \dots, N\}, \tag{3.11}$$

where $f^n := f(t^n)$ and $I : L^2(\Omega) \to V_{h0}$ is a computable interpolation or projection operator. This may be written in the following equivalent pointwise form: find $\{U^n\}_{n=1}^N \subset V_{h0}$ such that

$$\partial U^n - \mathcal{A}_h U^n = f_{h0}^n \quad \text{for all } \ n \in \{1, \dots, N\}, \tag{3.12}$$

where $f_{h0}^n = \mathcal{P}_0 f^n \in V_{h0}$.

3.3.2 *Crank–Nicolson time discretisation.* The Crank–Nicolson scheme for finding approximate solutions of (2.5) may be expressed as follows: given $U^0 = Iu_0$, find $\{U^n\}_{n=1}^N \subset V_{h0}$ satisfying

$$(\partial U^n, v_h) + \tfrac{1}{2} a(U^n + U^{n-1}, v_h) = (f^{n-\frac{1}{2}}, v_h) \quad \text{for all } v_h \in V_{h0} \text{ and } n \in \{1, \dots, N\}, \tag{3.13}$$

where $f^{n-\frac{1}{2}} = f\big(\frac{t^n + t^{n-1}}{2}\big)$. The equivalent pointwise form of this scheme is as follows: find $\{U^n\}_{n=1}^N \subset V_{h0}$ satisfying

$$\partial U^n - \tfrac{1}{2}\mathcal{A}_h U^n - \tfrac{1}{2}\mathcal{A}_h U^{n-1} = f_{h0}^{n-\frac{1}{2}} \quad \text{for all } \ n \in \{1, \dots, N\}, \tag{3.14}$$

where $f_{h0}^{n-\frac{1}{2}} = \mathcal{P}_0 f^{n-\frac{1}{2}} \in V_{h0}$.

4. *A posteriori* error estimation

To derive the $L^\infty(0, t; L^2(\Omega))$ error estimates for the backward Euler and Crank–Nicolson schemes of Theorem 4.11, we proceed in several stages. We begin in Section 4.1 by introducing the space, time and space-time reconstructions of the discrete solutions, which will be used to split the error into separate components. These allow us, in Section 4.2, to derive differential equations satisfied by the error that have controllable right-hand sides and thus form the basis of our error estimates. Some tools for producing error estimates composed of very flexible varieties of time accumulation are discussed in Sections 4.3 and 4.4; these are applied to the error equations of Section 4.2 to derive estimates on the parabolic component of the error. The final *a posteriori* error estimate is then built out of these components in Section 4.5. In Section 4.6 we briefly revisit each stage of the procedure to demonstrate how the additional error produced by allowing the spatial mesh to vary between time steps may be naturally incorporated into the present framework.

4.1 *Space and time reconstruction operators*

The forthcoming analysis rests on the use of various reconstructions of the solution in space and time, which we define here. We begin by defining the spatial reconstruction we use, which is the celebrated elliptic reconstruction operator of Makridakis & Nochetto (2003).

Definition 4.1 (Elliptic reconstruction). Let $\mathcal{R} : V_{h0} \times L^2(\Omega) \to H_0^1(\Omega)$ denote the *elliptic reconstruction operator* satisfying

$$a\big(\mathcal{R}(w_h, g), v\big) = \big(-\mathcal{A}_h w_h + \mathcal{P} g - \mathcal{P}_0 g, v\big) \qquad \text{for all } v \in H_0^1(\Omega). \tag{4.1}$$

Based on this construction we introduce the abbreviated notation $\mathcal{R}w_h := \mathcal{R}(w_h, 0)$.

The key property of the elliptic reconstruction operator is that any $w_h \in V_{h0}$ can now be seen as satisfying the finite element discretisation of the elliptic problem satisfied by $\mathcal{R}(w_h, g)$. This allows us to utilise the well-developed literature on *a posteriori* error estimates for elliptic problems (see, for example, Ainsworth & Oden, 2000; Brenner & Scott, 2008; Verfürth, 2013, etc.) in order to estimate quantities of the form $\|w_h - \mathcal{R}(w_h, g)\|$. To demonstrate this, in Lemma 4.2 we provide an example of a residual-type *a posteriori* error estimate, which may be proven using standard techniques. It is worth stressing that the choice of a residual-type bound here is by no means the only possibility—a great strength of the elliptic reconstruction technique is that any methodology for designing *a posteriori* estimates for elliptic problems can be applied here.

LEMMA 4.2 (Elliptic reconstruction error estimate). There exists a constant C_{ellip}, depending only on the domain Ω, the problem data, the polynomial degree k and the regularity of the mesh $\mathcal{T}_h$, such that for any $w_h \in V_{h0}$, the elliptic reconstruction operator $\mathcal{R}$ satisfies

$$\left\|w_h - \mathcal{R}(w_h, g)\right\| \leqslant \mathscr{E}(w_h, g) := C_{\text{ellip}}\left(\left\|h^2\left(\mathcal{A}_h w_h + \mathcal{P}_0 g - \mathcal{P}g - \mathcal{A}w_h\right)\right\|_{\mathcal{T}_h}^2 + \left\|h^{3/2}[\![A\nabla w_h]\!]\right\|_{\Gamma_h}^2\right)^{1/2}. \tag{4.2}$$

To define the time reconstructions that will also be required for the final error estimates we first introduce the so-called *temporal hat functions*, continuous piecewise linear functions $\ell^n : [0, T] \to [0, 1]$ for each $n = 0, \ldots, N$ satisfying $\ell^i(t^j) = \delta_{ij}$, where δ_{ij} is Kronecker's delta. These are defined as

$$\ell^n(t) = \begin{cases} \frac{t - t^{n-1}}{\tau_n} & \text{for } t \in \left[t^{n-1}, t^n\right], \\ \frac{t^{n+1} - t}{\tau_n} & \text{for } t \in \left[t^n, t^{n+1}\right], \\ 0 & \text{otherwise.} \end{cases} \tag{4.3}$$

Using these, we introduce the time and space-time approximations of the forcing data

$$f^\tau(t) = \sum_{n=0}^{N} f^n \ell^n(t), \qquad f_h(t) = \mathcal{P}f^\tau(t) \quad \text{and} \quad f_{h0}(t) = \mathcal{P}_0 f^\tau(t). \tag{4.4}$$

We next introduce time and space-time reconstructions of the nodal discrete solutions U^n provided by the discrete schemes, given in Definition 4.3. The quadratic reconstruction we adopt here is a slight simplification of the 'two-point reconstruction' studied by Akrivis *et al.* (2006), Lozinski *et al.* (2009) and Bänsch *et al.* (2012, 2013).

DEFINITION 4.3 (Time and space-time reconstructions). Let $\{U^n\}_{n=0}^N \subset V_{h0}$ denote the set of discrete approximate solutions produced by either the backward Euler or Crank–Nicolson scheme. We let $U, Q : [0, T] \to V_{h0}$ denote the *linear* and *quadratic time reconstructions*, given by

$$U(t) = \sum_{n=0}^{N} U^n \ell^n(t) \quad \text{and} \quad Q(t) = U(t) - \sum_{n=1}^{N} \frac{\tau_n^2}{2} \partial\left(\mathcal{A}_h U^n + f_{h0}^n\right) \ell^n(t) \ell^{n-1}(t), \tag{4.5}$$

respectively. We further let $U^{\mathcal{R}}, Q^{\mathcal{R}} : [0,T] \to H_0^1(\Omega)$ denote the *linear* and *quadratic space-time reconstructions*, given by

$$U^{\mathcal{R}}(t) = \mathcal{R}\big(U(t), f^\tau(t)\big) = \sum_{n=0}^{N} \mathcal{R}\big(U^n, f^n\big)\ell^n(t), \tag{4.6}$$

$$Q^{\mathcal{R}}(t) = \mathcal{R}\big(Q(t), f^\tau(t)\big) = U^{\mathcal{R}}(t) - \sum_{n=1}^{N} \frac{\tau_n^2}{2}\mathcal{R}\partial\big(\mathcal{A}_h U^n + f_{h0}^n\big)\ell^n(t)\ell^{n-1}(t), \tag{4.7}$$

respectively.

We remark that all of these reconstructions are continuous in time. Indeed, for each $n \in \{0,\dots,N\}$ the time reconstructions satisfy $U(t^n) = Q(t^n) = U^n$, while the space-time reconstructions satisfy $U^{\mathcal{R}}(t^n) = Q^{\mathcal{R}}(t^n) = \mathcal{R}(U^n, f^n)$.

4.2 *Error equations*

The final error estimate (Theorem 4.11) will be proven by splitting the error into components using the triangle inequality with the reconstructions of Definition 4.3 and controlling each term separately. For the backward Euler scheme this splitting is

$$\|u - U\|_{L^\infty(0,t;L^2(\Omega))} \leqslant \big\|u - U^{\mathcal{R}}\big\|_{L^\infty(0,t;L^2(\Omega))} + \big\|U^{\mathcal{R}} - U\big\|_{L^\infty(0,t;L^2(\Omega))}, \tag{4.8}$$

while for the Crank–Nicolson scheme the splitting is

$$\|u - U\|_{L^\infty(0,t;L^2(\Omega))} \leqslant \big\|u - Q^{\mathcal{R}}\big\|_{L^\infty(0,t;L^2(\Omega))} + \big\|Q^{\mathcal{R}} - Q\big\|_{L^\infty(0,t;L^2(\Omega))} + \|Q - U\|_{L^\infty(0,t;L^2(\Omega))}. \tag{4.9}$$

The first component in each case is known as the *parabolic error* and measures the error between the true solution u and the reconstruction. The focus of this section is to derive an appropriate *error equation*, a differential equation satisfied by the parabolic error, which will be used to bound the first term of each splitting. This is performed separately in Section 4.2.1 for the backward Euler scheme and in Section 4.2.2 for the Crank–Nicolson scheme. The second term of each splitting, known as the *space reconstruction error*, measures the difference between a discrete solution and its reconstruction, and may be bounded using Lemma 4.2. Finally, the third term of the Crank–Nicolson splitting measures the *time reconstruction error* and is bounded directly by using the definition of the quadratic time reconstruction.

4.2.1 *Backward Euler error equation.* Invoking the definition of the elliptic reconstruction the discrete solutions produced by the backward Euler scheme satisfy

$$\big(U_t(t), v\big) + a\big(U^{\mathcal{R}}(t^n), v\big) = \big(f_h^n, v\big) \qquad \text{for all } v \in H_0^1(\Omega). \tag{4.10}$$

We observe that the effect of including projections of the forcing data in the definition of the reconstruction is that the right-hand side of this differential equation no longer involves the projection of f onto functions with zero boundary data, a fact that is important for obtaining error estimates with optimal-order data approximation terms.

Subtracting (4.10) from the variational form (2.5) we deduce that the *backward Euler parabolic error* $\xi(t) := u(t) - U^{\mathcal{R}}(t)$ satisfies the error equation

$$(\xi_t, v) + a(\xi, v) = \big(U_t - U_t^{\mathcal{R}}, v\big) + a\big(U^{\mathcal{R}}(t^n) - U^{\mathcal{R}}, v\big) + \big(f - f_h^n, v\big) \tag{4.11}$$

for any $v \in H_0^1(\Omega)$.

The terms on the right-hand side of (4.11) may be controlled by the (computable) error estimator functionals given in Definition 4.4, as shown in Lemma 4.5. To keep the notation from becoming too obscure we denote each component of the estimator in a calligraphic font by the first letter of its name, with the subscript 'BE' to indicate that it relates to the backward Euler scheme.

Definition 4.4 (Terms of the backward Euler error estimate). Let $n \in \{1, \dots, N\}$ and $t \in [t^{n-1}, t^n]$. We define the *space error estimator* and *elliptic reconstruction error estimator* as

$$\mathcal{S}_{\mathrm{BE}}(t) = \mathscr{E}\big(U_t(t), f_t^\tau(t)\big) \quad \text{and} \quad \mathcal{E}_{\mathrm{BE}}(t) = \mathscr{E}\big(U(t), f^\tau(t)\big), \tag{4.12}$$

respectively, with $\mathscr{E}$ denoting the elliptic error estimator from Lemma 4.2, the *time error estimator* as

$$\mathcal{T}_{\mathrm{BE}}(t) = \tau_n \big\| \partial\big(\mathcal{A}_h^{U^n} - f_h^n + f_{h0}^n\big) \big\| \tag{4.13}$$

and the *data approximation error estimators* for *time* and *space* as

$$\mathcal{D}_{T,\mathrm{BE}}(t) = \big\| f(t) - f^n \big\| \qquad \text{and} \qquad \mathcal{D}_{S,\mathrm{BE}}(t) = C_{\mathrm{interp}} \big\| h\big(f^n - f_h^n\big) \big\|, \tag{4.14}$$

respectively.

Lemma 4.5 (Estimates for individual backward Euler error equation terms). Let $n \in \{1, \dots, N\}$ and $t \in [t^{n-1}, t^n]$. Then, for any $v \in H_0^1(\Omega)$, the terms of the backward Euler error equation (4.11) may be bounded with separate contributions from the spatial and temporal errors

$$\big(U_t(t) - U_t^{\mathcal{R}}(t), v\big) \leqslant \mathcal{S}_{\mathrm{BE}}(t)\|v\| \quad \text{and} \quad a\big(U^{\mathcal{R}}(t^n) - U^{\mathcal{R}}(t), v\big) \leqslant \mathcal{T}_{\mathrm{BE}}(t)\|v\|, \tag{4.15}$$

respectively, and the data approximation error

$$\big(f(t) - f_h^n, v\big) \leqslant \mathcal{D}_{T,BE}(t)\|v\| + \mathcal{D}_{S,BE}(t)|||v|||. \tag{4.16}$$

Proof. Observing that $U_t^{\mathcal{R}}(t) = \mathcal{R}(U_t(t), f_t^\tau(t))$, the first term on the right-hand side of (4.11) is bounded by applying the Cauchy–Schwarz inequality and Lemma 4.2. Since $\ell^{n-1}(t) = 1 - \ell^n(t)$ for $t \in [t^{n-1}, t^n]$ the second term of (4.11) may be rewritten as

$$a\big(U^{\mathcal{R}}(t^n) - U^{\mathcal{R}}, v\big) = \ell^{n-1}(t) a\big(\mathcal{R}\big(U^n, f^n\big) - \mathcal{R}\big(U^{n-1}, f^{n-1}\big), v\big) \tag{4.17}$$

$$= -\tau_n \ell^{n-1}(t)\big(\partial\big(\mathcal{A}_h U^n + f_{h0}^n - f_h^n\big), v\big), \tag{4.18}$$

and the result follows by applying the Cauchy–Schwarz inequality and using the fact that $\ell^{n-1}(t) \leqslant 1$.

The final term of (4.11) may be bounded by adding and subtracting f^n, recalling that $f_h^n = \mathcal{P}f^n$ and exploiting the $L^2(\Omega)$ orthogonality of the projector $\mathcal{P}$ to introduce the Clément interpolant $v_h \in V_{h0}$ of v, providing

$$\big(f - f_h^n, v\big) = \big(f - f^n, v\big) + \big(f^n - f_h^n, v - v_h\big). \tag{4.19}$$

The result then follows by applying the Cauchy–Schwarz inequality and the bounds of Lemma 3.1. □

4.2.2 *Crank–Nicolson error equation.* The definition of the quadratic time reconstruction Q, given in (4.5), ensures that it satisfies the differential equation

$$Q_t(t) - \mathcal{A}_h U(t) = f_{h0}(t) + \Big(f_{h0}^{n-\frac{1}{2}} - f_{h0}\Big(t^{n-\frac{1}{2}}\Big)\Big), \tag{4.20}$$

where $f_{h0}(t) = \mathcal{P}_0 f_h(t)$, and the construction of the elliptic reconstruction operator therefore implies

$$\big(Q_t(t), v\big) + a\big(U^{\mathcal{R}}(t), v\big) = \big(f_h(t), v\big) + \Big(f_{h0}^{n-\frac{1}{2}} - f_{h0}\Big(t^{n-\frac{1}{2}}\Big), v\Big) \qquad \text{for all } v \in H_0^1(\Omega). \tag{4.21}$$

Taken together, the variational form (2.5) and relation (4.21) imply that the *Crank–Nicolson parabolic error* $\rho(t) := u(t) - Q^{\mathcal{R}}(t)$ satisfies the error equation

$$(\rho_t, v) + a(\rho, v) = \big(Q_t - Q_t^{\mathcal{R}}, v\big) + a\big(U^{\mathcal{R}} - Q^{\mathcal{R}}, v\big) + \big(f - f_h, v\big) + \Big(f_{h0}^{n-\frac{1}{2}} - f_{h0}\Big(t^{n-\frac{1}{2}}\Big), v\Big) \tag{4.22}$$

for any $v \in H_0^1(\Omega)$.

The terms on the right-hand side of (4.22) may be controlled by the error estimator functionals defined in Definition 4.6, as shown in Lemma 4.7. Once again, we denote each of the estimators in a calligraphic font by the first letter of its name, this time with the subscript 'CN' to indicate that it relates to the Crank–Nicolson scheme.

DEFINITION 4.6 (Terms of the Crank–Nicolson error estimate). Let $n \in \{1, \dots, N\}$ and $t \in [t^{n-1}, t^n]$. We define the *space error estimator* and *elliptic reconstruction error estimator* as

$$\mathcal{S}_{\mathrm{CN}}(t) = \mathscr{E}\big(Q_t(t), f_t^\tau(t)\big) \quad \text{and} \quad \mathcal{E}_{\mathrm{CN}}(t) = \mathscr{E}\big(Q(t), f^\tau(t)\big), \tag{4.23}$$

respectively, where $\mathscr{E}$ is the elliptic error estimator from Lemma 4.2, the *time error estimator* as

$$\mathcal{T}_{\mathrm{CN}}(t) = C_{\mathrm{interp}} \frac{\tau_n^2}{8} \Big(\big|\!\big| \big| \partial\big(\mathcal{A}_h U^n + f_{h0}^n\big) \big|\!\big| + \big\| h\mathcal{A}_h \partial\big(\mathcal{A}_h U^n + f_{h0}^n\big) \big\| \Big), \tag{4.24}$$

the *quadratic time reconstruction estimator* as

$$\mathcal{Q}_{\mathrm{CN}}(t) = \frac{\tau_n^2}{8} \big\| \partial\big(\mathcal{A}_h U^n + f_{h0}^n\big) \big\| \tag{4.25}$$

and the *data approximation error estimators* for *time* and *space* as

$$\mathcal{D}_{T,\mathrm{CN}}(t) = \left\| f(t) - f^{\tau}(t) \right\| + \left\| f_{h0}^{n-\frac{1}{2}} - f_{h0}\left(t^{n-\frac{1}{2}}\right) \right\| \quad \text{and} \quad \mathcal{D}_{S,\mathrm{CN}}(t) = C_{\mathrm{interp}} \left\| h\left(f^{\tau}(t) - f_h(t)\right) \right\|, \tag{4.26}$$

respectively.

Lemma 4.7 (Estimates for individual Crank–Nicolson error equation terms). The terms of the Crank–Nicolson error equation (4.22) may be bounded with separate contributions from the spatial and temporal errors

$$\left(Q_t(t) - Q_t^{\mathcal{R}}(t), v\right) \leqslant \mathcal{S}_{\mathrm{CN}}(t)\|v\| \quad \text{and} \quad a\left(U^{\mathcal{R}}(t) - Q^{\mathcal{R}}(t), \rho\right) \leqslant \mathcal{T}_{\mathrm{CN}}(t)|||v|||, \tag{4.27}$$

respectively, and the data approximation error

$$\left(f(t) - f_h(t), v\right) + \left(f_{h0}^{n-\frac{1}{2}} - f_{h0}\left(t^{n-\frac{1}{2}}\right), v\right) \leqslant \mathcal{D}_{T,CN}(t)\|v\| + \mathcal{D}_{S,CN}(t)|||v|||. \tag{4.28}$$

Proof. The estimates for the space and data approximation errors are broadly similar to the estimates given in Lemma 4.5, so are omitted. For the bound on the time error we first observe that

$$a\left(U^{\mathcal{R}} - Q^{\mathcal{R}}, v\right) = \frac{\tau_n^2}{2} \ell^n(t)\ell^{n-1}(t) a\left(\mathcal{R}\partial\left(\mathcal{A}_h U^n + f_{h0}^n\right), v\right). \tag{4.29}$$

Letting $v_h \in V_{h0}$ denote the Clément interpolant of v we obtain

$$a\left(\mathcal{R}\partial\left(\mathcal{A}_h U^n + f_{h0}^n\right), v\right) = a\left(\mathcal{R}\partial\left(\mathcal{A}_h U^n + f_{h0}^n\right), v - v_h\right) + a\left(\mathcal{R}\partial\left(\mathcal{A}_h U^n + f_{h0}^n\right), v_h\right) \tag{4.30}$$

$$= -\left(\mathcal{A}_h\partial\left(\mathcal{A}_h U^n + f_{h0}^n\right), v - v_h\right) + a\left(\partial\left(\mathcal{A}_h U^n + f_{h0}^n\right), v_h\right). \tag{4.31}$$

The result then follows from the continuity of a, the approximation and stability properties of the Clément interpolant laid out in Lemma 3.1 and the fact that $\ell^n(t)\ell^{n-1}(t) \leqslant \frac{1}{4}$. □

4.3 *Time accumulations*

We now introduce some machinery that will be required to derive a wide variety of new error estimates. We first introduce the *accumulation weighting coefficients*, nondecreasing bounded functions of time that control the rate at which error accumulates and have a significant effect on the estimate at early times, as demonstrated in Section 5.

Definition 4.8 (Accumulation weighting coefficients). Let $p \in [1, \infty]$, $\lambda \in [0, 1]$ and $r \in (0, T]$. We introduce the *accumulation weighting coefficients*

$$c_{p,r} := \|\beta_r\|_{L^q(0,r)} = \begin{cases} \left(\dfrac{1 - e^{-q\alpha_\lambda r}}{q\alpha_\lambda}\right)^{1/q} & \text{for } p \in (1, \infty], \\ 1 & \text{for } p = 1, \end{cases} \tag{4.32}$$

where q satisfies $\frac{1}{p} + \frac{1}{q} = 1$, $\beta_r(s) = e^{\alpha_\lambda(s-r)}$ and $\alpha_\lambda = \frac{2(1-\lambda)}{(\gamma C_{\mathrm{PF}})^2}$.

We note that the coefficients $c_{p,r}$ are non-decreasing continuous functions of r, and continuous functions of p. The rationale for introducing these accumulation weighting coefficients is demonstrated by Lemma 4.9. Here one should think of the term F as representing some estimator term accumulating with the simulation time and v as the error that we are trying to bound (either in the $L^\infty(L^2)$ or a weighted $L^2(H^1)$ norm). The terms being bounded in each case are typical terms that we shall encounter in the subsequent error analysis; cf. Lemma 4.10.

LEMMA 4.9 (Exponentially weighted time accumulations). Let $r > 0$ and suppose that $F \in L^\infty(0,r)$, with $F(t) \geqslant 0$ for a.e. $t \in [0,r]$. Then for $v \in L^\infty(0,r;L^2(\Omega))$ the estimate

$$\int_0^r e^{\alpha_\lambda(s-r)}F(s)\|v(s)\|\,\mathrm{d}s \leqslant \min_{p\in[1,\infty]} c_{p,r}\|F\|_{L^p(0,r)} \max_{s\in[0,r]}\|v(s)\| \tag{4.33}$$

holds, and for $v \in L^2(0,r;H^1(\Omega))$ the estimate

$$\int_0^r e^{\alpha_\lambda(s-r)}F(s)|||v(s)|||\,\mathrm{d}s \leqslant \min_{p\in[2,\infty]} \left(c_{\frac{p}{2},r}\right)^{1/2}\|F\|_{L^p(0,r)} \left(\int_0^r e^{\alpha_\lambda(s-r)}|||v(s)|||^2\,\mathrm{d}s\right)^{1/2} \tag{4.34}$$

holds. The accumulation weighting coefficients $c_{p,r}$ are defined in Definition 4.8.

Proof. We begin by proving (4.33). Taking the maximum of $\|v(t)\|$ and applying Hölder's inequality for some $p \in [1,\infty]$ we find

$$\int_0^r e^{\alpha_\lambda(s-r)}F(s)\|v(s)\|\,\mathrm{d}s \leqslant \max_{s\in[0,t^m]}\|v(s)\| \int_0^r e^{\alpha_\lambda(s-r)}F(s)\,\mathrm{d}s \leqslant \|\beta_r\|_{L^q(0,r)}\|F\|_{L^p(0,r)} \max_{s\in[0,t^m]}\|v(s)\|, \tag{4.35}$$

where $\beta_r(t) = e^{\alpha_\lambda(t-r)}$ and q satisfies $\frac{1}{p}+\frac{1}{q}=1$. Taking the infimum over the (arbitrary) parameter $p \in [1,\infty]$ we observe that this infimum is attained since the set $[1,\infty]$ is closed and the estimate is continuous with respect to p; it follows that the infimum is thus a minimum. The result then follows by noting that $c_{p,r} = \|\beta_r\|_{L^q(0,r)}$ by definition.

To prove (4.34) we argue similarly. Applying the Cauchy–Schwarz inequality we find

$$\int_0^r e^{\alpha_\lambda(s-r)}F(s)|||v(s)|||\,\mathrm{d}s \leqslant \left(\int_0^r e^{\alpha_\lambda(s-r)}|||v(s)|||^2\,\mathrm{d}s\right)^{1/2}\left(\int_0^r e^{\alpha_\lambda(s-r)}(F(s))^2\,\mathrm{d}s\right)^{1/2}. \tag{4.36}$$

Hölder's inequality, applied to the second term for some $p \in [1,\infty]$, then implies

$$\left(\int_0^r e^{\alpha_\lambda(s-r)}(F(s))^2\,\mathrm{d}s\right)^{1/2} \leqslant \|\beta_r\|^{1/2}_{L^q(0,r)}\|F\|_{L^{2p}(0,r)}, \tag{4.37}$$

where q once again satisfies $\frac{1}{p}+\frac{1}{q}=1$. The result then follows as before from the definition of $c_{p,r}$ and the fact that p is arbitrary. □

A few comments on this result are in order at this point. First, we note that the result may be extended to the case when F is only in $L^p(0,r)$ for $p < \infty$, although we present the proof for the case of

$F \in L^\infty(0,r)$ for clarity. In the case when F is constant on each interval, say $F(t) = F^n \geqslant 0$ on $t \in (t^{n-1}, t^n)$, then the accumulation becomes

$$\|F\|_{L^p(0,t^m)} = \begin{cases} \left(\sum_{n=1}^m \tau_n \left(F^n\right)^p\right)^{1/p} & \text{for } p \in [1,\infty), \\ \max_{n\in\{1,\dots,m\}} F^n & \text{for } p = \infty, \end{cases} \tag{4.38}$$

which, for $p = 1, 2$, yields the time accumulations familiar from conventional $L^\infty(0,T;L^2(\Omega))$ error estimates such as those in Lakkis & Makridakis (2006), Lozinski *et al.* (2009), Bänsch *et al.* (2012, 2013), Karakatsani (2012) and Georgoulis *et al.* (2017), for instance.

We next observe that while both bounds (4.33) and (4.34) allow for L^∞-type time accumulations of F, only the former supports L^1-type accumulations. As we shall demonstrate in Section 5, L^1-type accumulations are generally preferable for short-time estimates. In most situations one has a choice of which of the terms bounded in Lemma 4.9 will appear in the error equation, the latter often coming with an extra power of h (for instance, observe the bound of the data approximation term in Lemma 4.10). In this light, the choice may be seen as an alternative perspective on the conventional trade-off between powers of h or τ. Since the aim of this work is to present *long*-time estimates we shall not trouble ourselves too much on this point, although it is worth bearing in mind.

Finally, we remark that it is possible to subdivide the domain $[0,r]$ used in Lemma 4.9 and apply different types of accumulations on each subdivision. For instance, if $r_0 = 0$, $r_M = r$ and $r_{i-1} < r_i$ for $i = 1,\dots,M$, we could obtain a bound of the form

$$\int_0^r e^{\alpha_\lambda(s-r)} F(s)\|v(s)\|\,\mathrm{d}s \leqslant \max_{s\in[0,r]} \|v(s)\| \sum_{i=1}^M \left(\min_{p_i\in[1,\infty]} c_{p_i,[r_{i-1},r_i]} \|F\|_{L^{p_i}(r_{i-1},r_i)} \right), \tag{4.39}$$

where, here only, we use the notation $c_{p,[a,b]} = \|\beta_r\|_{L^q(a,b)}$ for $a, b \in [0,r]$, with β_r and q defined as in Definition 4.8. It is clear that this bound is sharper than the bound (4.33) and could allow very general error estimates. In the interests of clarity, however, this is not something we pursue any further here.

4.4 *Estimates for the parabolic error*

We now draw together the tools of Lemmas 4.5, 4.7 and 4.9 to provide an estimate for the parabolic error in each scheme. While Lemmas 4.5 and 4.7 provided spatial estimates for individual terms, in some sense, this result provides a temporal estimate and is the key point of departure in the proof from conventional $L^\infty(L^2)$ error estimates as it is here that the new varieties of time accumulation appear. The first step of the argument, in which a Poincaré–Friedrichs inequality is applied, is a well-known technique for deriving *a priori* error estimates for this class of problem, cf. Thomée (2006), and appears to have been first applied in an *a posteriori* setting in a slightly different way to ultimately derive the final-time $L^2(\Omega)$ error estimate of Lakkis *et al.* (2015, Section 6).

LEMMA 4.10 ($L^\infty(0,t;L^2(\Omega))$ parabolic error estimates). For any $r \in (0,T]$ the backward Euler parabolic error ξ and Crank–Nicolson parabolic error ρ satisfy

$$\max_{s\in[0,r]}\|\xi(s)\| \leqslant \|\xi(0)\| + \sqrt{2}\Bigg(\min_{p\in[1,\infty]} c_{p,r}\|\mathcal{S}_{\mathrm{BE}}\|_{L^p(0,r)} + \min_{p\in[1,\infty]} c_{p,r}\|\mathcal{T}_{\mathrm{BE}}\|_{L^p(0,r)} + \min_{p\in[1,\infty]} c_{p,r}\|\mathcal{D}_{T,BE}\|_{L^p(0,r)} + \min_{p\in[2,\infty]} \left(c_{\frac{p}{2},r}\right)^{1/2}\|\mathcal{D}_{S,\mathrm{BE}}\|_{L^p(0,r)}\Bigg) \tag{4.40}$$

and

$$\max_{s\in[0,r]}\|\rho(s)\| \leqslant \|\rho(0)\| + \sqrt{2}\Bigg(\min_{p\in[1,\infty]} c_{p,r}\|\mathcal{S}_{\mathrm{CN}}\|_{L^p(0,r)} + \min_{p\in[2,\infty]} \left(c_{\frac{p}{2},r}\right)^{1/2}\|\mathcal{T}_{\mathrm{CN}}\|_{L^p(0,r)} + \min_{p\in[1,\infty]} c_{p,r}\|\mathcal{D}_{T,\mathrm{CN}}\|_{L^p(0,r)} + \min_{p\in[2,\infty]} \left(c_{\frac{p}{2},r}\right)^{1/2}\|\mathcal{D}_{S,\mathrm{CN}}\|_{L^p(0,r)}\Bigg), \tag{4.41}$$

respectively. The accumulation weighting coefficients $c_{p,r}$ used here are defined in Definition 4.8.

Proof. We prove the Crank–Nicolson estimate, and the backward Euler estimate follows similarly.

To begin we select $v = \rho$ in (4.22) and apply the estimates of Lemma 4.7 to the terms on the right-hand side individually. We therefore find that, for any $n \in \{1,\dots,N\}$ and $t \in [t^{n-1}, t^n]$,

$$\frac{1}{2}\frac{d}{dt}\|\rho(t)\|^2 + |||\rho(t)|||^2 \leqslant \Big(\mathcal{S}_{\mathrm{CN}}(t) + \mathcal{D}_{T,\mathrm{CN}}(t)\Big)\|\rho(t)\| + \Big(\mathcal{T}_{\mathrm{CN}}(t) + \mathcal{D}_{S,\mathrm{CN}}(t)\Big)|||\rho(t)|||. \tag{4.42}$$

The Poincaré–Friedrichs inequality and the norm equivalence (2.4) imply that, for any $\lambda \in [0,1]$,

$$\frac{1}{2}\frac{d}{dt}\|\rho(t)\|^2 + \alpha\|\rho(t)\|^2 + \lambda|||\rho(t)|||^2 \leqslant \frac{1}{2}\frac{\mathrm{d}}{\mathrm{d}t}\|\rho(t)\|^2 + |||\rho(t)|||^2, \tag{4.43}$$

where we denote $\alpha := \alpha_\lambda = \frac{2(1-\lambda)}{(\gamma C_{\mathrm{PF}})^2}$ (as in Definition 4.8; we omit the subscript for brevity), and therefore

$$\frac{1}{2}\frac{\mathrm{d}}{\mathrm{d}t}\Big(e^{\alpha t}\|\rho(t)\|^2\Big) + \lambda e^{\alpha t}|||\rho(t)|||^2 \leqslant e^{\alpha t}\Big(\mathcal{S}_{\mathrm{CN}}(t) + \mathcal{D}_{T,\mathrm{CN}}(t)\Big)\|\rho(t)\| + e^{\alpha t}\Big(\mathcal{T}_{\mathrm{CN}}(t) + \mathcal{D}_{S,\mathrm{CN}}(t)\Big)|||\rho(t)|||. \tag{4.44}$$

Integrating over $[0,r]$, we thus obtain

$$\frac{1}{2}\|\rho(r)\|^2 + \lambda\int_0^r e^{\alpha(s-r)}|||\rho(s)|||^2\,\mathrm{d}s \leqslant \frac{1}{2}e^{-\alpha r}\|\rho(0)\|^2 + \int_0^r e^{\alpha(s-r)}\Big(\mathcal{S}_{\mathrm{CN}}(s) + \mathcal{D}_{T,\mathrm{CN}}(s)\Big)\|\rho(s)\| + e^{\alpha(s-r)}\Big(\mathcal{T}_{\mathrm{CN}}(s) + \mathcal{D}_{S,\mathrm{CN}}(s)\Big)|||\rho(s)|||\,\mathrm{d}s. \tag{4.45}$$

Invoking Lemma 4.9 with $v = \rho$ on each term of the integral and observing that $e^{-\alpha r} \leqslant 1$ provides

$$\begin{aligned}\frac{1}{2}\|\rho(r)\|^2 + \lambda \int_0^r e^{\alpha(s-r)} |||\rho(s)|||^2 \,\mathrm{d}s \qquad (4.46)\\ \leqslant \frac{1}{2}\|\rho(0)\|^2 + \max_{s\in[0,r]} \|\rho(s)\| \left(\min_{p\in[1,\infty]} c_{p,r} \|\mathcal{S}_{\mathrm{CN}}\|_{L^p(0,r)} + \min_{p\in[1,\infty]} c_{p,r} \|\mathcal{D}_{T,\mathrm{CN}}\|_{L^p(0,r)} \right)\\ + \left(\int_0^r e^{\alpha(s-r)} |||\rho(s)|||^2 \,\mathrm{d}s \right)^{1/2} \left(\min_{p\in[2,\infty]} (c_{\frac{p}{2},r})^{1/2} \|\mathcal{T}_{\mathrm{CN}}\|_{L^p(0,r)} + \min_{p\in[2,\infty]} \left(c_{\frac{p}{2},r}\right)^{1/2} \|\mathcal{D}_{S,\mathrm{CN}}\|_{L^p(0,r)} \right).\end{aligned}$$

We next apply Young's inequality, which states that if $a, b \geqslant 0$, then $ab \leqslant \frac{\epsilon}{2}a^2 + \frac{1}{2\epsilon}b^2$ for any $\epsilon > 0$. Picking $\epsilon = 2\lambda$ and applying the inequality to the final two factors of the bound therefore produces

$$\begin{aligned}\frac{1}{2}\|\rho(r)\|^2 \leqslant \frac{1}{2}\|\rho(0)\|^2 + \max_{s\in[0,r]} \|\rho(s)\| \left(\min_{p\in[1,\infty]} c_{p,r} \|\mathcal{S}_{\mathrm{CN}}\|_{L^p(0,r)} + \min_{p\in[1,\infty]} c_{p,r} \|\mathcal{D}_{T,\mathrm{CN}}\|_{L^p(0,r)} \right)\\ + \frac{1}{4\lambda} \left(\min_{p\in[2,\infty]} \left(c_{\frac{p}{2},r}\right)^{1/2} \|\mathcal{T}_{\mathrm{CN}}\|_{L^p(0,r)} + \min_{p\in[2,\infty]} \left(c_{\frac{p}{2},r}\right)^{1/2} \|\mathcal{D}_{S,\mathrm{CN}}\|_{L^p(0,r)} \right)^2. \qquad (4.47)\end{aligned}$$

We note that a function of the form $\min_{p\in[1,\infty]} c_{p,r}\|F\|_{L^p(0,r)}$ is nondecreasing with respect to r. This is because the function is nondecreasing for each value of p (due to the properties of the $L^p(0,r)$ norm), and we are therefore taking the minimum over a set of nondecreasing functions. Since the right-hand side of this estimate is thus a sum of terms which are each nondecreasing functions of r, it follows that it too is a nondecreasing function of r, and we therefore deduce that (4.47) also provides a bound on $\max_{s\in[0,r]} \|\rho(s)\|^2$. The result then follows by applying Young's inequality once again, taking square roots and selecting $\lambda = \frac{1}{4}$. □

We note that it is necessary to apply Hölder's inequality (in the guise of Lemma 4.9) in the proof of Lemma 4.10 before one may derive a bound for $\max_{s\in[0,r]} \|\rho(s)\|$. This is because a quantity of the form

$$G(r) = \int_0^r e^{\alpha_\lambda (s-r)} |g(s)| \,\mathrm{d}s \qquad (4.48)$$

can be a *decreasing* function of r, since the exponential weight in the integral possesses a 'forgetfulness' property: for fixed s the function $e^{\alpha_\lambda(s-r)}$ decreases as r increases. Hence, as r increases, less weight is assigned to the early part of the integral and $G(r)$ can therefore decrease. This means that an estimate of the form of G is well suited for a final-time estimate (cf. Lakkis *et al.*, 2015, Section 6), although not for a maximum norm estimate. Upon applying Hölder's inequality, however, this problem is alleviated since the exponential weight and the function g are integrated separately.

4.5 *Final error estimates*

Finally, we are in a position to provide optimal-order estimates for the $L^\infty(0,t;L^2(\Omega))$ error for the backward Euler and Crank–Nicolson schemes. These are based on using the splittings (4.8) and (4.9) of the error and applying the estimates of Lemmas 4.2 and 4.10 for each component.

THEOREM 4.11 ($L^\infty(0,t;L^2(\Omega))$ error estimates). Let $r \in (0,T]$. If $\{U^n\}_{n=0}^N$ denotes the backward Euler approximations of u at the time nodes, then

$$\begin{aligned}\|u-U\|_{L^\infty(0,r;L^2(\Omega))} \leqslant{}& \|u_0 - Iu_0\| + \|\mathcal{E}_{\mathrm{BE}}\|_{L^\infty(0,r)} \\ &+ \sqrt{2}\Bigg(\min_{p\in[1,\infty]} c_{p,r}\|\mathcal{S}_{\mathrm{BE}}\|_{L^p(0,r)} + \min_{p\in[1,\infty]} c_{p,r}\|\mathcal{T}_{\mathrm{BE}}\|_{L^p(0,r)} \\ &+ \min_{p\in[1,\infty]} c_{p,r}\|\mathcal{D}_{T,\mathrm{BE}}\|_{L^p(0,r)} + \min_{p\in[2,\infty]} \left(c_{\frac{p}{2},r}\right)^{1/2}\|\mathcal{D}_{S,\mathrm{BE}}\|_{L^p(0,r)}\Bigg),\end{aligned} \tag{4.49}$$

where the individual terms are defined in Definition 4.4.

If $\{U^n\}_{n=0}^N$ denotes the Crank–Nicolson approximations of u at the time nodes, then

$$\begin{aligned}\|u-U\|_{L^\infty(0,r;L^2(\Omega))} \leqslant{}& \|u_0 - Iu_0\| + \|\mathcal{E}_{\mathrm{CN}}\|_{L^\infty(0,r)} + \|\mathcal{Q}_{\mathrm{CN}}\|_{L^\infty(0,r)} \\ &+ \sqrt{2}\Bigg(\min_{p\in[1,\infty]} c_{p,r}\|\mathcal{S}_{\mathrm{CN}}\|_{L^p(0,r)} + \min_{p\in[2,\infty]} \left(c_{\frac{p}{2},r}\right)^{1/2}\|\mathcal{T}_{\mathrm{CN}}\|_{L^p(0,r)} \\ &+ \min_{p\in[1,\infty]} c_{p,r}\|\mathcal{D}_{T,\mathrm{CN}}\|_{L^p(0,r)} + \min_{p\in[2,\infty]} \left(c_{\frac{p}{2},r}\right)^{1/2}\|\mathcal{D}_{S,\mathrm{CN}}\|_{L^p(0,r)}\Bigg),\end{aligned} \tag{4.50}$$

where the individual terms are defined in Definition 4.6. The accumulation weighting coefficients $c_{p,r}$ used here are defined in Definition 4.8.

Proof. For the backward Euler scheme we utilise the splitting (4.8) and apply Lemmas 4.10 and 4.2 to the two terms respectively to provide the desired result. Similarly, for the Crank–Nicolson scheme, we use the splitting (4.9) and apply Lemmas 4.10 and 4.2 to the first two terms respectively, and we observe that, for $t \in (t^{n-1}, t^n]$,

$$Q(t) - U(t) = -\frac{\tau_n^2}{2}\ell^n(t)\ell^{n-1}(t)\partial\left(\mathcal{A}_h U^n + f_{h0}^n\right), \tag{4.51}$$

so that $\|Q-U\| \leqslant \mathcal{Q}_{\mathrm{CN}}$, and the result follows. □

4.6 *The effects of mesh modification*

We conclude this section by briefly demonstrating that the effects of mesh modification may be incorporated into the present framework of general time accumulations in an identical manner to that of previous related error estimates (see, for instance, the estimate of Lakkis & Makridakis, 2006 for backward Euler schemes and Bänsch *et al.*, 2012, 2013 for Crank–Nicolson schemes). To keep technicalities to a minimum we demonstrate this only for the backward Euler scheme.

Since the mesh may now vary between time steps we shall denote by $\mathscr{T}_h^n$ the mesh of Ω at time step n and the finite element space with respect to this mesh by V_h^n, with $V_{h0}^n = V_h^n \cap H_0^1(\Omega)$. We suppose that the mesh $\mathscr{T}_h^n$ is obtained from the mesh $\mathscr{T}_h^{n-1}$ by a finite number of coarsening or refinement operations. Let $\mathcal{I}^n : V_h^{n-1} \to V_h^n$ denote a computable *mesh transfer operator* (for instance, this could be a Lagrangian interpolant or the $L^2(\Omega)$-orthogonal projection operator).

Introducing the *transferred* discrete time derivative operator $\widehat{\partial}^n : V_h^n \to V_h^n$, defined for a set of functions $\{w_h^n\}_{n=0}^N$ with $w_h^n \in V_h^n$ by

$$\widehat{\partial}^n w_h^n := \frac{w_h^n - \mathcal{I}^n w_h^{n-1}}{\tau_n} \tag{4.52}$$

(as before, we shall use the shorthand notation $\widehat{\partial} = \widehat{\partial}^n$ for brevity), we are able to present the *backward Euler scheme with mesh modification*: given $U^0 = Iu_0$, find $\{U^n\}_{n=1}^N$ with $U^n \in V_{h0}^n$ satisfying

$$\big(\widehat{\partial} U^n, v^n\big) + a\big(U^n, v^n\big) = \big(f^n, v^n\big) \quad \text{for all } v^n \in V_{h0}^n \text{ and } n \in \{1, \dots, N\}. \tag{4.53}$$

Denoting the discrete spatial operator on the space V_{h0}^n by $\mathcal{A}_h^n$, defined as in (3.7), and the $L^2(\Omega)$-orthogonal projection operators onto V_h^n and V_{h0}^n by $\mathcal{P}^n$ and $\mathcal{P}_0^n$, respectively, defined analogously to those in (3.8), we observe that the numerical scheme may be written in the equivalent pointwise form

$$\widehat{\partial} U^n - \mathcal{A}_h^n U^n = f_{h0}^n \quad \text{for all } n \in \{1, \dots, N\}, \tag{4.54}$$

analogous to (3.12), where in this case we denote $f_h^n = \mathcal{P}^n f$ and $f_{h0}^n = \mathcal{P}_0^n f$.

This motivates the following redefinition of the space-time approximations of f:

$$f_h(t) = \sum_{n=0}^N f_h^n \ell^n(t) \quad \text{and} \quad f_{h0}(t) = \sum_{n=0}^N f_{h0}^n \ell^n(t), \tag{4.55}$$

and a time-step-dependent elliptic reconstruction operator $\mathcal{R}^n : V_{h0}^n \times L^2(\Omega) \to H_0^1(\Omega)$, satisfying

$$a\big(\mathcal{R}^n\big(w^n, g\big), v\big) = \big(- \mathcal{A}_h^n w^n + \mathcal{P}^n g - \mathcal{P}_0^n g, v\big) \qquad \text{for all } v \in H_0^1(\Omega). \tag{4.56}$$

With the time reconstruction $U(t)$ defined as in Definition 4.3, we use this to modify the definition of the space-time reconstruction to

$$U^{\mathcal{R}}(t) = \sum_{n=0}^N \mathcal{R}^n\big(U^n, f^n\big)\ell^n(t) \tag{4.57}$$

for $t \in (t^{n-1}, t^n)$, and we thus find that the parabolic error $\xi(t) = u(t) - U^{\mathcal{R}}(t)$ satisfies the error equation

$$(\xi_t, v) + a(\xi, v) = \big(U_t - U_t^{\mathcal{R}}, v\big) + \big(U_t - \widehat{\partial} U^n, v\big) + a\big(U^{\mathcal{R}}(t^n) - U^{\mathcal{R}}, v\big) + \big(f - f_h^n, v\big) \tag{4.58}$$

for all $v \in H_0^1(\Omega)$. The new term here is the second one; previously, the construction of $U(t)$ ensured that this was zero, although in the present setting we find that this provides a *mesh transfer error estimator*: for $t \in (t^{n-1}, t^n)$,

$$\|U_t(t) - \widehat{\partial} U^n\| = \tau_n^{-1} \|U^{n-1} - \mathcal{I}^n U^{n-1}\| =: \mathcal{M}_{\mathrm{ABE}}(t). \tag{4.59}$$

The treatment of the first term of (4.58) is also a little more involved in this case, although the compatibility assumed on the sequence of meshes ensures that the following result may be proven by arguing as in Lakkis & Makridakis (2006, §3.6).

LEMMA 4.12 (Two mesh spatial error estimate). Let $n \in \{1, \dots, N\}$, suppose that $t \in (t^{n-1}, t^n)$ and let $\hat{h}(x) = \max(h^n(x), h^{n-1}(x))$. Let $\mathscr{T}_h^n \vee \mathscr{T}_h^{n-1}$ denote the *coarsest common refinement mesh* of $\mathscr{T}_h^n$ and $\mathscr{T}_h^{n-1}$, which may be formed by applying the refinement operations to $\mathscr{T}_h^{n-1}$ which would be used to construct $\mathscr{T}_h^n$, but not the coarsening operations. Then

$$\begin{aligned}\left\|\left(U - U^{\mathcal{R}}\right)_t(t)\right\| \leqslant \mathcal{S}_{\mathrm{ABE}}(t) := C_{\mathrm{ellip}}\Big(&\|\hat{h}^2\big(\mathcal{A}U_t(t) - \left(\mathcal{A}_h U - f_{h0} + f_h\right)_t(t)\big)\|^2_{\mathscr{T}_h^n \vee \mathscr{T}_h^{n-1}} \\ &+ \|\hat{h}^{3/2}[\![A\nabla U_t(t)]\!]\|^2_{\Gamma_h^n \cup \Gamma_h^{n-1}}\Big)^{1/2}.\end{aligned} \tag{4.60}$$

Here we have adopted the (abuse of) notation

$$\mathcal{A}_h U(t) := \sum_{n=0}^{N} \mathcal{A}_h^n U^n \ell^n(t). \tag{4.61}$$

We observe that if $\mathscr{T}_h^n = \mathscr{T}_h^{n-1}$, then $\mathcal{S}_{\mathrm{ABE}}(t) = \mathcal{S}_{\mathrm{BE}}(t)$. Treating the remaining terms of the error equation (4.58) as before we therefore derive the following analogue of Lemma 4.5.

LEMMA 4.13 (Estimates for individual error equation terms). Let $n \in \{1, \dots, N\}$ and $t \in [t^{n-1}, t^n]$. Then, for any $v \in H_0^1(\Omega)$, the terms of the backward Euler error equation (4.58) may be bounded with separate contributions from the spatial and temporal errors,

$$\left(U_t(t) - U_t^{\mathcal{R}}(t), v\right) \leqslant \mathcal{S}_{\mathrm{ABE}}(t)\|v\| \quad \text{and} \quad a\left(U^{\mathcal{R}}(t^n) - U^{\mathcal{R}}(t), v\right) \leqslant \mathcal{T}_{\mathrm{BE}}(t)\|v\|, \tag{4.62}$$

respectively, and the data approximation and mesh transfer errors,

$$(f(t) - f_h^n, v) \leqslant \mathcal{D}_{T,\mathrm{BE}}(t)\|v\| + \mathcal{D}_{S,\mathrm{BE}}(t)|||v||| \quad \text{and} \quad (U_t(t) - \widehat{\partial} U^n, v) \leqslant \mathcal{M}_{\mathrm{ABE}}(t)\|v\|, \tag{4.63}$$

respectively. The estimators $\mathcal{T}_{\mathrm{BE}}(t), \mathcal{D}_{T,\mathrm{BE}}(t)$ and $\mathcal{D}_{S,\mathrm{BE}}(t)$ are defined in Definition 4.4.

Following the (mesh-independent) arguments of Sections 4.4 and 4.5 we finally obtain the following full error estimate.

THEOREM 4.14 ($L^\infty(0,T;L^2(\Omega))$ error estimate for the backward Euler scheme with mesh modification). Let $r \in (0,T]$. If $\{U^n\}_{n=0}^N$ denotes the approximations of u at the time nodes obtained through the backward Euler scheme with mesh modification (4.53), then

$$\begin{aligned}\|u - U\|_{L^\infty(0,r;L^2(\Omega))} \leqslant \|u_0 - Iu_0\| + \|\mathcal{E}_{\mathrm{BE}}\|_{L^\infty(0,r)} \\ + \sqrt{2}\Big(&\min_{p\in[1,\infty]} c_{p,r}\|\mathcal{S}_{\mathrm{ABE}}\|_{L^p(0,r)} + \min_{p\in[1,\infty]} c_{p,r}\|\mathcal{T}_{\mathrm{BE}}\|_{L^p(0,r)} \\ &+ \min_{p\in[1,\infty]} c_{p,r}\|\mathcal{M}_{\mathrm{ABE}}\|_{L^p(0,r)} + \min_{p\in[1,\infty]} c_{p,r}\|\mathcal{D}_{T,\mathrm{BE}}\|_{L^p(0,r)} \\ &+ \min_{p\in[2,\infty]} (c_{\frac{p}{2},r})^{1/2}\|\mathcal{D}_{S,\mathrm{BE}}\|_{L^p(0,r)}\Big).\end{aligned} \tag{4.64}$$

The accumulation weighting coefficients $c_{p,r}$ used here are defined in Definition 4.8.

5. Numerical experiments

In this section we present some numerical experiments demonstrating the practical behaviour of the estimators. We begin with an investigation into the different types of time accumulations, before considering approximating solutions to certain benchmark problems. To produce the results presented here the schemes and estimators described above were implemented using the open source `deal.II` finite element library (Bangerth *et al.*, 2007).

5.1 *Comparison of accumulations*

First, consider the accumulation of a term F such that $F^n = 1$ for all n. In this case, for $p \in [1, \infty)$, we have

$$\|F\|^p_{L^p(0,t^m)} = \sum_{n=1}^{m} \tau_n (F^n)^p = \sum_{n=1}^{m} \tau_n = t^m, \tag{5.1}$$

and $\|F\|_{L^\infty(0,t^m)} = 1$. It is clear, therefore, that for finite values of p the accumulation will grow unboundedly with t^m, while for $p = \infty$ the value will remain constant. Despite this, for $t^m < 1$, the choice $p = 1$ clearly provides the smallest accumulation. Thus, we find that

$$\min_{p\in[1,\infty]} \|F\|_{L^p(0,t^m)} = \begin{cases} t^m & \text{when } t^m \leqslant 1, \\ 1 & \text{otherwise,} \end{cases} \tag{5.2}$$

implying that the L^1-type accumulation is best for short-time computations (i.e., with $T \leqslant 1$), while the L^∞-type accumulation is best for long-time computations.

The situation is different, however, if we include the accumulation weighting coefficients $c_{p,t}$, introduced in Definition 4.8. In this case the growth of the different weighted accumulations $c_{p,t}\|F\|_{L^p(0,t)}$ is depicted in Fig. 1, under the supposition that the constant $\alpha_\lambda = 1$. Figure 1(a) shows the growth of the different accumulations in the case when $F^n = 1$ for all n, and in this case it appears that the weighting coefficients have a levelling effect, in that the L^∞-type accumulation is always the smallest. This is no longer true in the more practically relevant situation when F^n varies randomly in the interval $[0, 10]$, depicted in Fig. 1(b). In this case it is still clear that the L^1-type accumulation grows much larger than the others, while the L^∞-type accumulation grows the slowest. The actual minimum, however, appears to be somewhere in between and changes throughout the time interval. For much longer times, however, it is expected that the minimum will ultimately be the L^∞-type accumulation, which in this case is known to be bounded above by 10.

Figure 1(c) shows the accumulations applied to the same data set but with $F^1 = 30$. This makes little difference to the L^1-type accumulation, although it has a dramatic effect for larger values of p. In such a situation, therefore, the L^∞-type accumulation will not be minimal until t becomes very large. Instead, in this situation it may be preferable to use a combination of different accumulation types on different subintervals of the time domain, as described in Section 4.3.

5.2 *Implementing L^p-type accumulations*

To evaluate the estimator using the optimal accumulation for each term we note that it is possible to store the contributions to each term from each time step and then implement a numerical optimisation procedure to systematically find the optimal value of p. However, such an algorithm would be expensive in terms of both memory (to store the data from every time step) and computation (to find the minimal

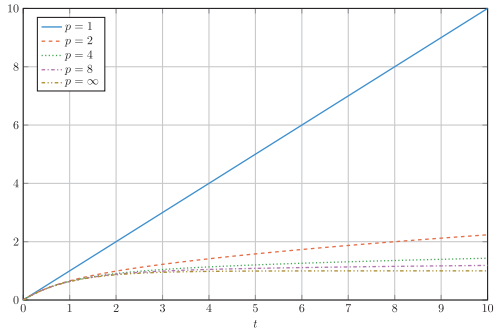

(a) $F^n = 1$ for all n.

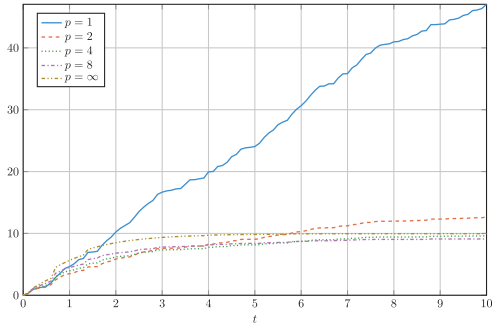

(b) F^n specified randomly in $[0, 10]$.

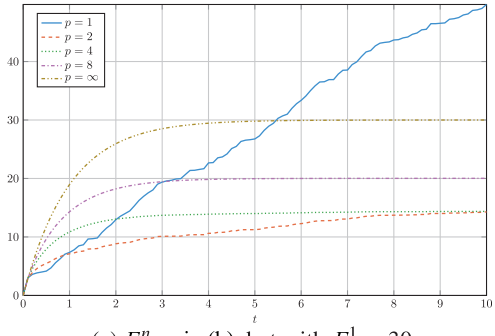

(c) F^n as in (b), but with $F^1 = 30$.

FIG. 1. The behaviour of the accumulations $c_{p,t}\|F\|_{L^p(0,t)}$ for different data F^n and various indicative values of p, with $\tau_n = 0.1$.

accumulation). Instead, we propose to evaluate the estimator using just a small number of accumulations for each term, for instance for $p \in \{1, 2, 4, 8, 16, \infty\}$. Computing the estimator like this requires storing only six numbers, as the degree p accumulation can be updated on each step using the update rule

$$\|F\|_{L^p(0,t^n)} = \begin{cases} \left(\|F\|^p_{L^p(0,t^{n-1})} + \tau_n \, (F^n)^p\right)^{1/p} & \text{for } p \in [1, \infty), \\ \max\{\|F\|_{L^p(0,t^{n-1})}, F^n\} & \text{for } p = \infty. \end{cases} \tag{5.3}$$

This is the approach taken for evaluating such terms in all of the numerical experiments presented below.

5.3 *Benchmark numerical examples*

We now investigate the behaviour of the estimator when applied to a sequence of example problems. For these examples we take A to be the $d \times d$ identity matrix and $\mu = 0$. The results are computed over the domain $\Omega = (0,1) \times (0,1)$ with $T = 15$, using a sequence of progressively finer meshes consisting of uniform square elements and polynomial degree $k = 1$. Unless otherwise stated, the mesh sequence consists of meshes with 2^{2i} elements, where $i \in \{2,3,4,5,6\}$. The mesh size may therefore be computed in each case as $h_i = 2^{1/2-2i}$.

For each example problem on each sequence of meshes we plot a composite figure of the resulting data. Subfigure (a) of each demonstrates the behaviour of the $L^\infty(0,t;L^2(\Omega))$ error and the total estimator, computed by taking the minimum of a subset of the accumulations as described in Section 5.2, with the simulation on each mesh being shown as a separate line on the plot (solid lines indicate the results computed on the finest mesh). Beneath each of these we plot the convergence rate with respect to i as a function of time, computed for a quantity F^i by

$$\text{rate}_i(t) = \frac{\log(F^i(t)) - \log(F^{i-1}(t))}{\log(h_i) - \log(h_{i-1})}. \tag{5.4}$$

Since the time step τ_i is a specified function of h_i in each case, this provides a meaningful definition of convergence rate. Next to these we plot the effectivity of the estimator, computed as

$$\text{effectivity}_i(t) = \frac{\text{estimator}_i(t)}{\|u - U_i\|_{L^\infty(0,t;L^2(\Omega))}}. \tag{5.5}$$

Here $\text{estimator}_i(t)$ and $U_i(t)$ denote the estimator and discrete solution calculated on mesh i.

Subfigure (b) of each plot shows the magnitudes and convergence rates of each component of the error estimator, computed using the minimal accumulation in each case. Finally, subfigure (c) in each case shows a comparison between the estimators evaluated using various specified types of accumulation. The line marked 'L^1 accumulations' shows the value of the estimator when all components are evaluated using L^p-type accumulations with the least admissible value of p in each case (for some terms this is 1, for others it is 2 or ∞). Similarly, the line 'L^2 accumulations' shows the behaviour where p is taken as value 2 for all components and the line 'L^∞ accumulations' shows the effect of taking $p = \infty$. To the right of these we plot the effectivity computed for each of these three estimators.

5.3.1 *Sinusoidal benchmark.*

We consider the problem with the solution

$$u(t,x,y) = \sin(\pi t)\sin(\pi x)\sin(\pi y). \tag{5.6}$$

For this example, we show results for the backward Euler scheme with time steps linked to the spatial discretisation as $\tau_i = h_i^2$ and $\tau_i = h_i$ in Figs 3 and 4, respectively, and for the Crank–Nicolson scheme with $\tau_i = h_i$ and $\tau_i = h_i^{1/2}$ in Figs 5 and 6, respectively. Since *a priori* error estimates inform us that the $L^\infty(0,t;L^2(\Omega))$ norm of the error should converge with order $\mathcal{O}(\tau + h^2)$ for the backward Euler scheme and with order $\mathcal{O}(\tau^2 + h^2)$ for the Crank–Nicolson scheme, we deduce that the expected convergence rates for the four simulations should be 2, 1, 2 and 1, respectively. For the Crank–Nicolson scheme with $\tau_i = h_i^{1/2}$, we include additional data for $i \in \{7,8\}$ in order to better demonstrate the asymptotic behaviour of the estimator.

Examining the plots in subfigure (a) for each figure indicates that these rates are attained by the true error, while the estimator seems to converge slightly faster on the coarser meshes for both of the cases when the expected rate is 1 (Figs 4 and 6). Since this appears to be settling down towards the expected rates on the finer meshes, this quirk is presumably attributable to some pre-asymptotic effects. This behaviour could be due to the fact that we are ignoring the values of the constants weighting each term of the estimator, meaning that the spatial estimators (which converge more quickly) initially dominate over the temporal estimators, which are responsible for restricting the total estimate to order 1. This pre-asymptotic behaviour observed in Figs 4 and 6 also has an impact on the effectivities of the estimator, which are significantly larger on coarser meshes than on finer meshes in the sequence. In Figs 3 and 6, however, where the error is expected to converge at rate 2, the estimator converges much more similarly to the error, resulting in effectivities that do not depend so much on the mesh.

What is striking in all four figures, though, is that the effectivities become *constant* with respect to time. This is entirely due to the use of the L^∞-type accumulations in the estimator, as shown by the plots in subfigure (c) in each case. The estimators making use of the L^1- and L^2-type accumulations grow much faster than the actual error. This is best demonstrated by Fig. 2, in which the data from the effectivity comparison of Fig. 6(c) is replotted on logarithmic axes. It becomes evident from this that, after an initial period in which the accumulation weighting coefficient dominates the profile of each curve, the effectivity of the L^1-type estimator grows like t, the L^2-type estimator's effectivity grows like $t^{1/2}$ and the L^∞-type estimator becomes constant.

5.3.2 *Polynomial benchmark.* We consider a problem with the solution

$$u(t,x,y) = \frac{x(x-1)y(y-1)}{250} t(t-2)(t-4)(t-6)(t-8)(t-10), \tag{5.7}$$

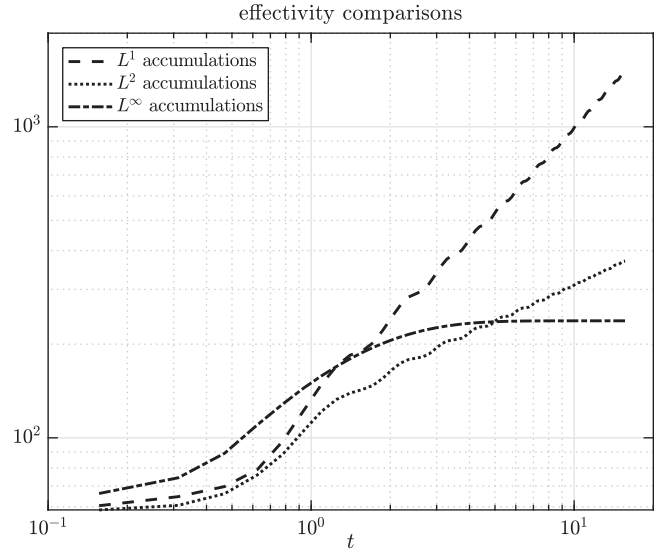

FIG. 2. The effectivity comparison of Fig. 5(c) replotted on logarithmic axes, revealing the asymptotic rates at which the different effectivities grow.

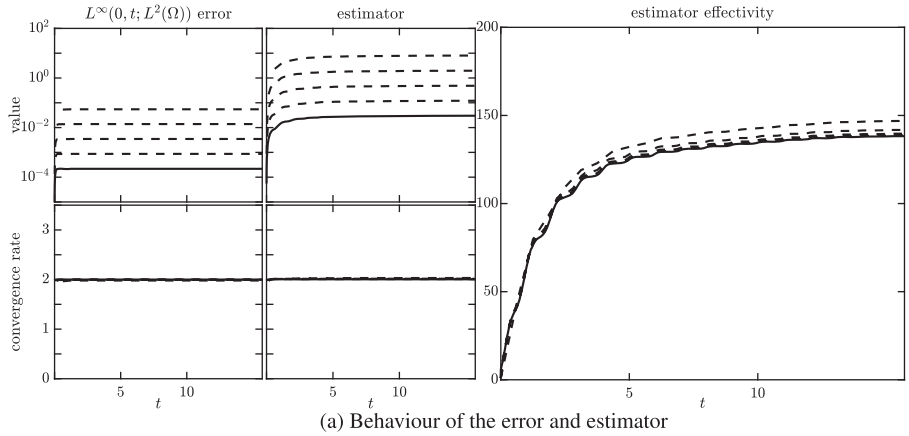

(a) Behaviour of the error and estimator

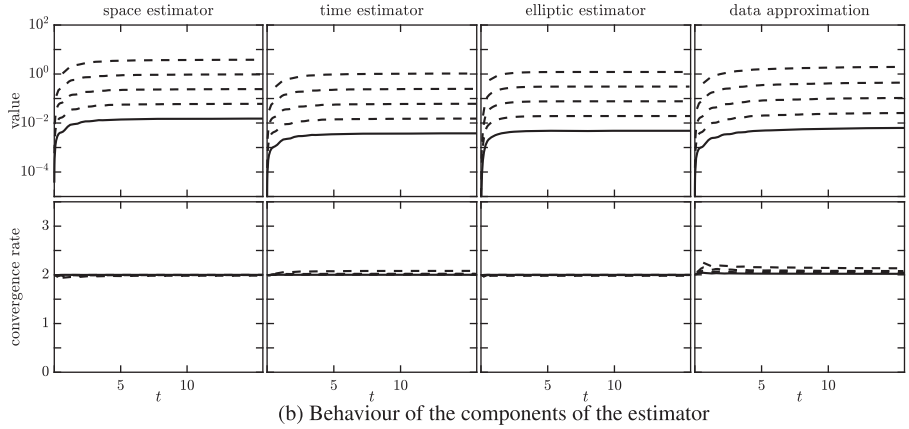

(b) Behaviour of the components of the estimator

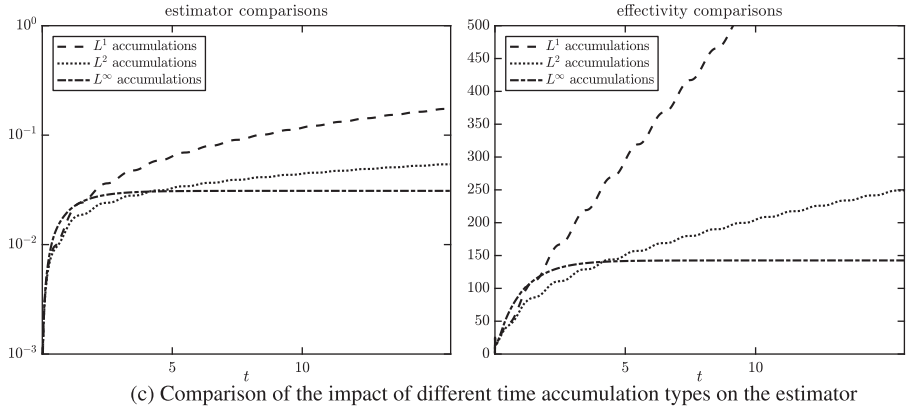

(c) Comparison of the impact of different time accumulation types on the estimator

FIG. 3. Behaviour of the error and estimator for the backward Euler scheme applied to the sinusoidal example (5.6) with $\tau \approx h^2$. Solid lines indicate results on the finest mesh.

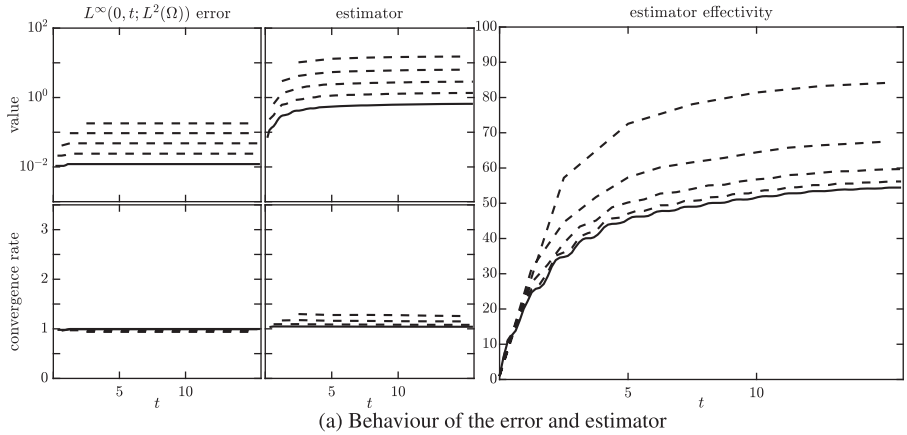

(a) Behaviour of the error and estimator

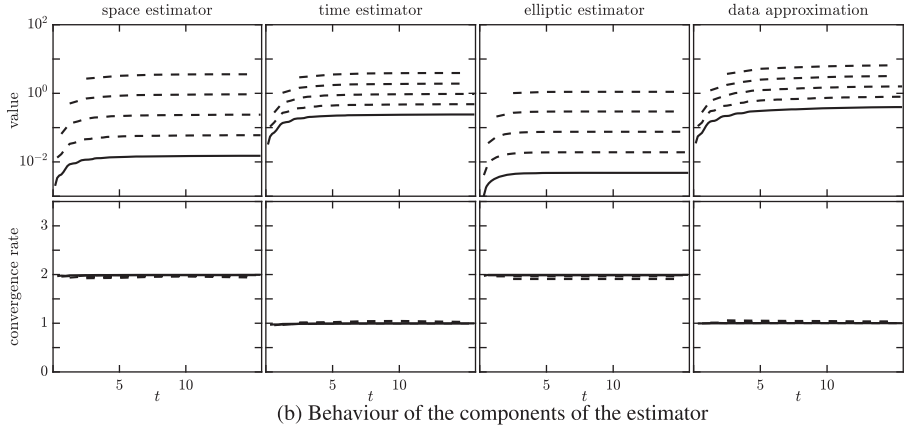

(b) Behaviour of the components of the estimator

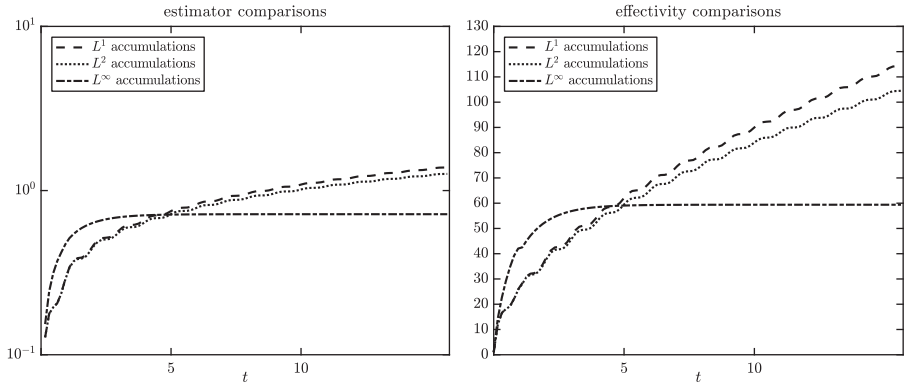

(c) Comparison of the impact of different time accumulation types on the estimator

FIG. 4. Behaviour of the error and estimator for the backward Euler scheme applied to the sinusoidal example (5.6) with $\tau \approx h$. Solid lines indicate results on the finest mesh.

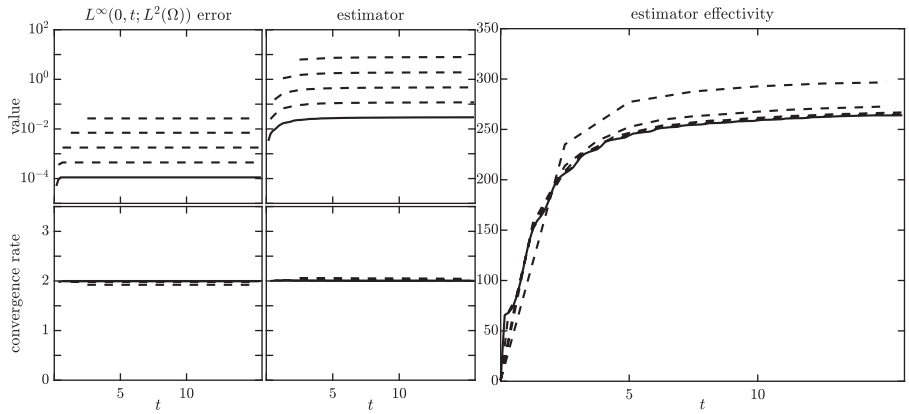

(a) Behaviour of the error and estimator

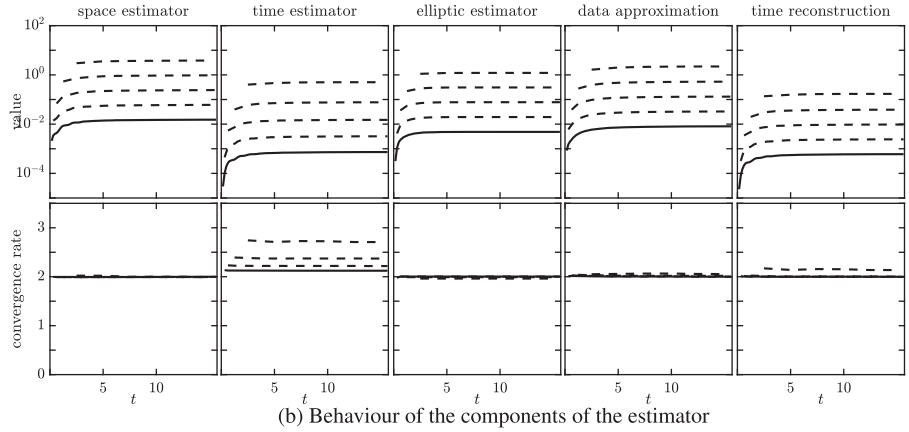

(b) Behaviour of the components of the estimator

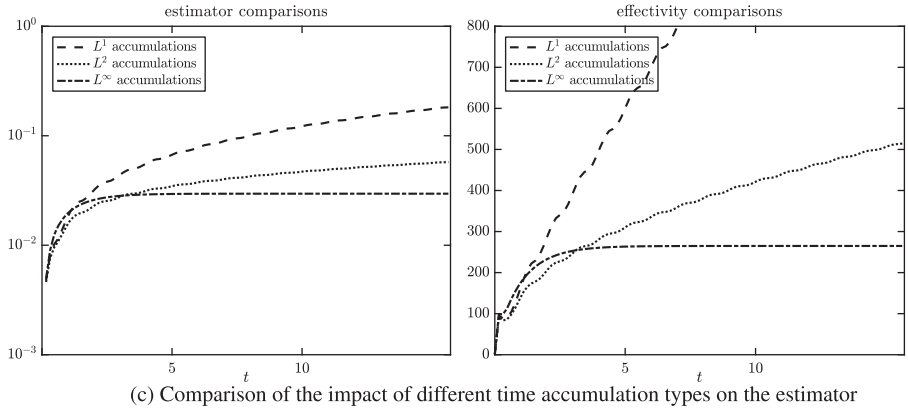

(c) Comparison of the impact of different time accumulation types on the estimator

FIG. 5. Behaviour of the error and estimator for the Crank–Nicolson scheme applied to the sinusoidal example (5.6) with $\tau \approx h$. Solid lines indicate results on the finest mesh.

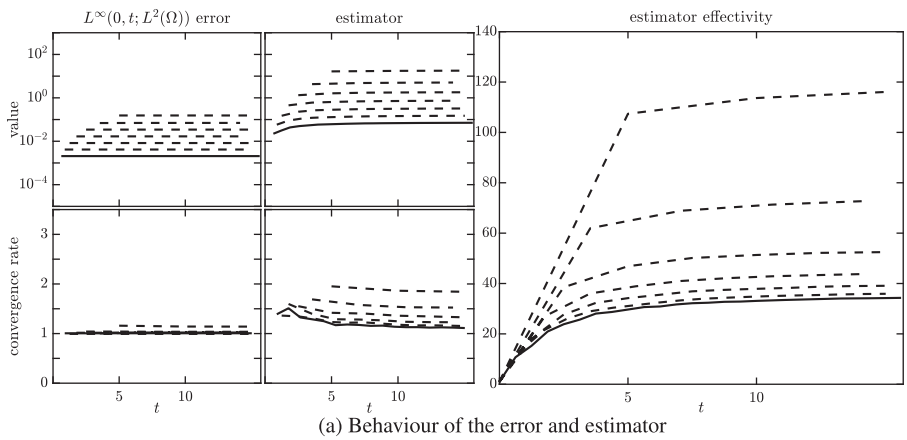

(a) Behaviour of the error and estimator

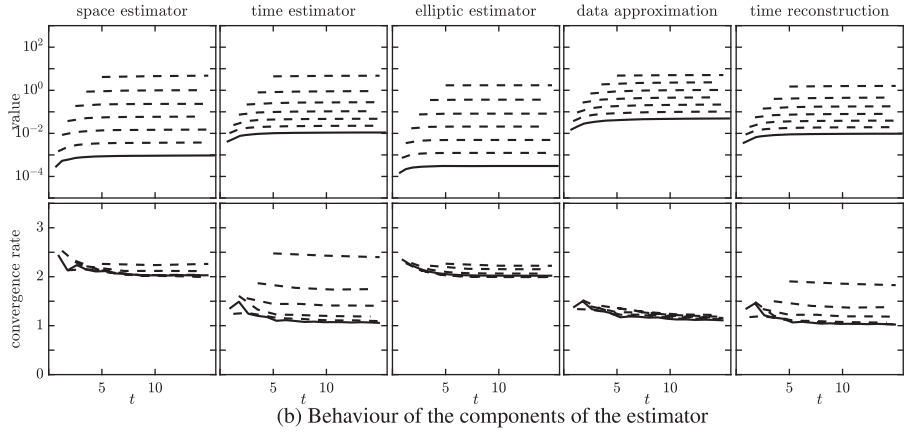

(b) Behaviour of the components of the estimator

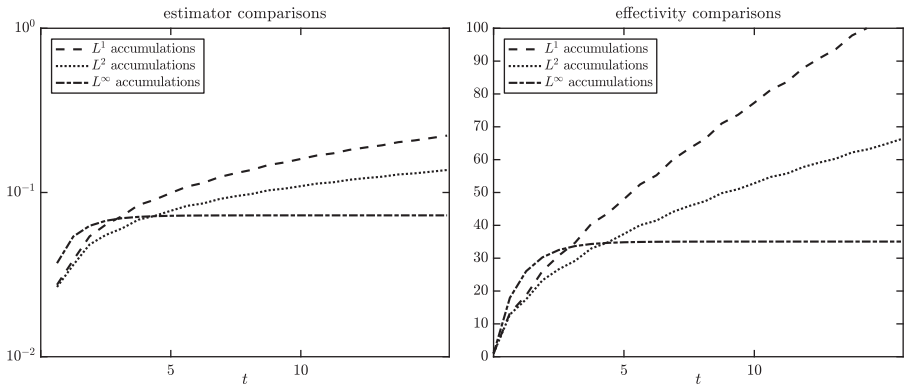

(c) Comparison of the impact of different time accumulation types on the estimator

FIG. 6. Behaviour of the error and estimator for the Crank–Nicolson scheme applied to the sinusoidal example (5.6) with $\tau \approx \sqrt{h}$. Solid lines indicate results on the finest mesh.

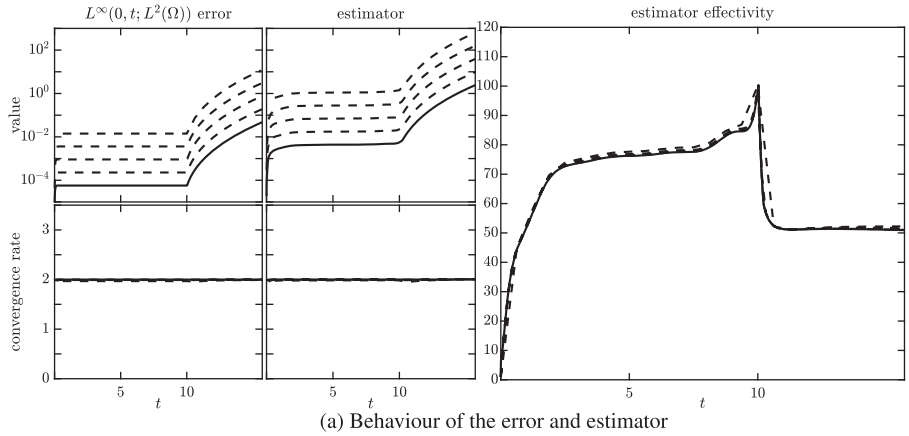

(a) Behaviour of the error and estimator

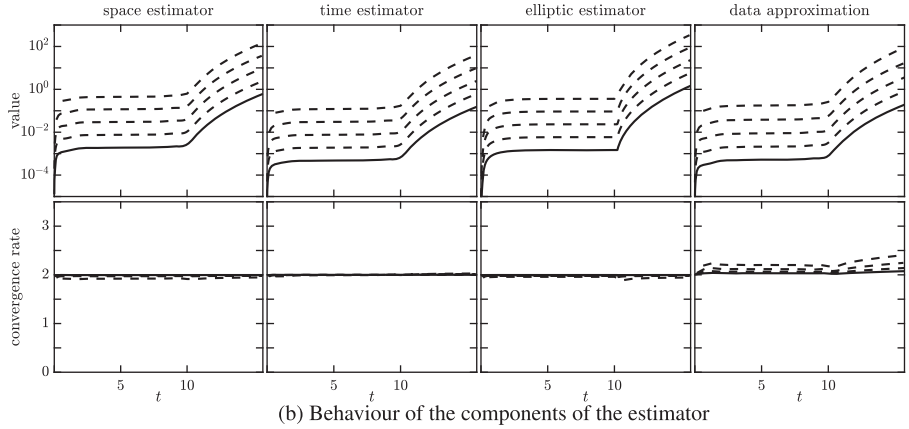

(b) Behaviour of the components of the estimator

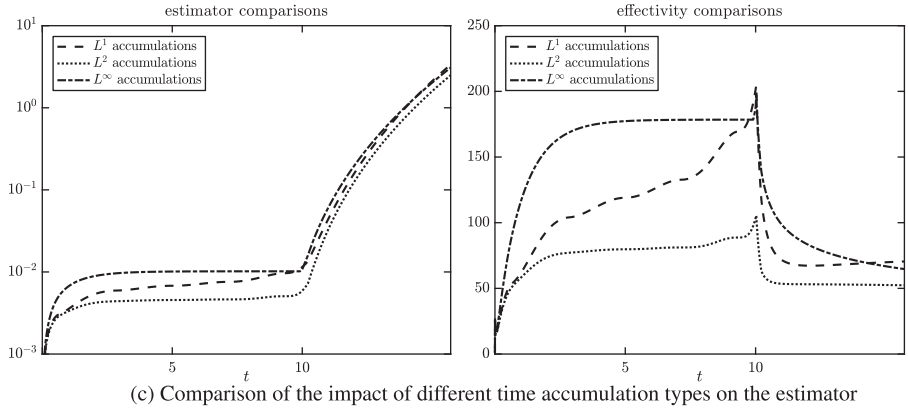

(c) Comparison of the impact of different time accumulation types on the estimator

FIG. 7. Behaviour of the error and estimator for the backward Euler scheme applied to the sinusoidal example (5.7) with $\tau \approx h^2$. Solid lines indicate results on the finest mesh.

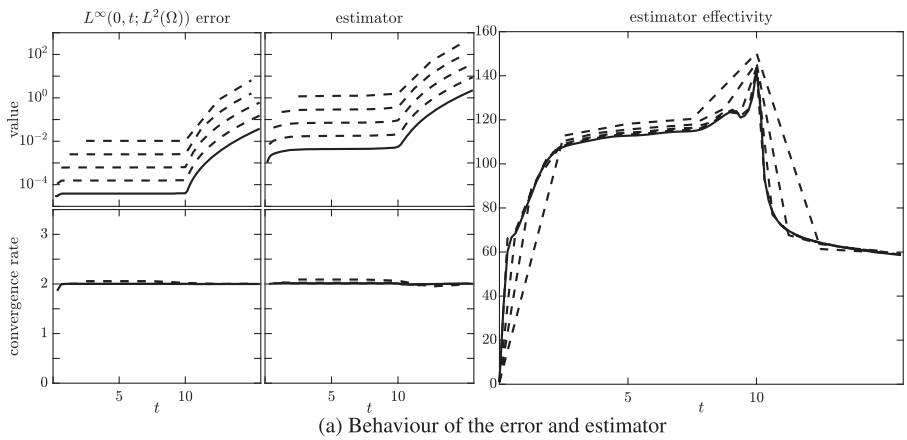

(a) Behaviour of the error and estimator

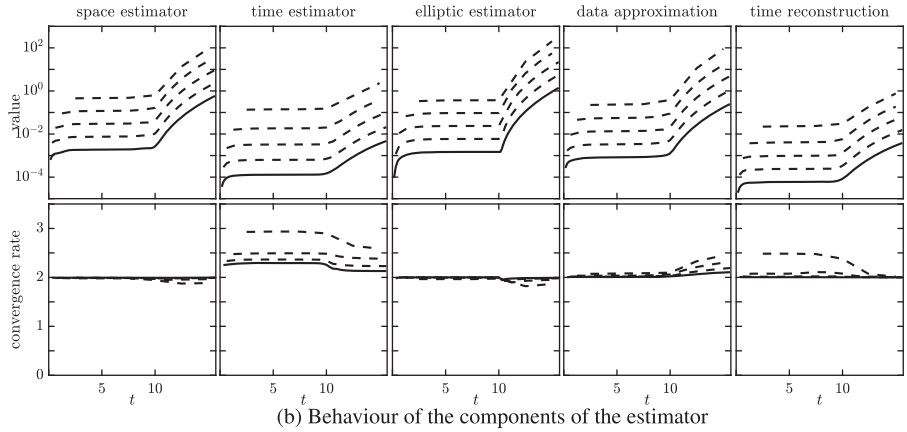

(b) Behaviour of the components of the estimator

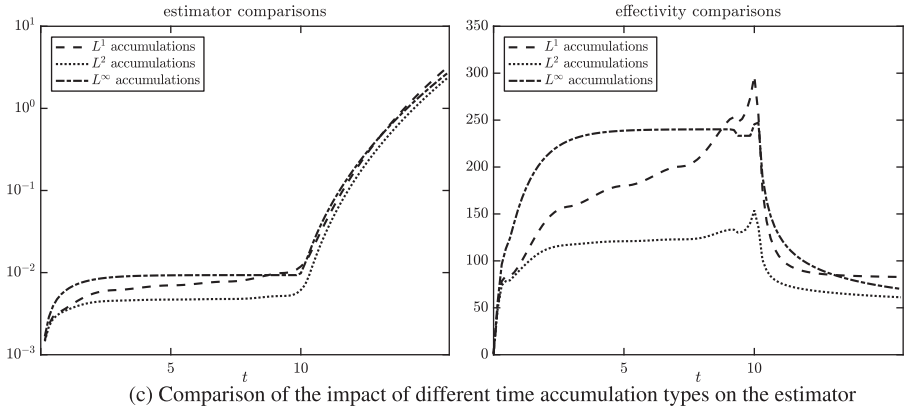

(c) Comparison of the impact of different time accumulation types on the estimator

FIG. 8. Behaviour of the error and estimator for the Crank–Nicolson scheme applied to the sinusoidal example (5.7) with $\tau \approx h$. Solid lines indicate results on the finest mesh.

which satisfies the problem with forcing term

$$f(t,x,y) = \frac{x(x-1)+y(y-1)}{125} t(t-2)(t-4)(t-6)(t-8)(t-10). \tag{5.8}$$

We note that for $t \in [0,10]$, $\max_{(x,y)\in\Omega} u(t,x,y)$ oscillates within $[-0.3, 0.1]$, but the solution grows so rapidly when $t \in [10,15]$ that $\max_{(x,y)\in\Omega} u(15,x,y) = 42{,}230$. The interesting features of this benchmark problem are therefore twofold: first, the forcing function is nonzero on $\partial\Omega$; secondly, we are interested to see how the estimator behaves with the rapid growth in the solution.

The results obtained from the backward Euler and Crank–Nicolson schemes applied to this problem are shown in Figs 7 and 8, respectively. To address the first point we observe that all components of both estimators remain of at least optimal order due to the modified definition of the elliptic reconstruction operator. The second point is more interesting. We observe that the effectivities of both estimators are relatively well behaved, remaining around 100. However, from the comparison of the estimators and effectivities obtained using different types of accumulation, we observe that in neither case is it optimal to use the L^∞-type accumulations; rather, L^2-type accumulations seem to behave best. Broadly speaking, this can be attributed to the fact that the error is large early on in the simulation, as in case (c) of Section 5.1, so the L^1- and L^2-type accumulations are preferable early on, while the contribution to the error on each time step grows for $t > 10$, ensuring that the L^∞-type accumulations also grow. We note that this could be a situation in which it is preferable to use different types of accumulation on different sections of the time domain, as discussed in Section 4.3.

6. Conclusions

In summary, we have derived a family of new optimal-order estimates for the $L^\infty(0,t;L^2(\Omega))$ norm error of finite element discretisations with backward Euler and Crank–Nicolson time-stepping schemes for a class of parabolic problems. The estimates in this family are almost all new and allow the individual terms of the estimator to accumulate through time in an $L^p(0,t)$ fashion for any $p \in [1,\infty]$. Included in this spectrum are, of course, previously known estimates relying on L^1- or L^2-type time accumulations of their terms, which we have demonstrated to exhibit effectivities (the ratio of the estimator to the true error) that grow like t or $\sqrt{t}$, respectively, where t is the simulation duration. Estimators based on L^∞-type accumulations were previously derived using parabolic duality-based techniques, although the derivation of analogous estimates using energy arguments remained an open question. The advantage of using L^∞-type accumulations is that the estimators attain constant effectivities on benchmark problems, meaning they are much better suited as error estimates for long-time simulations and offer potential for deriving lower bounds on the error.

The technique used to derive these estimates is fundamentally based on the structure of the partial differential equation, rather than the construction of the numerical scheme. To ensure the details of the new technique remain clear we have demonstrated the technique for finite element discretisations of linear parabolic problems with backward Euler and Crank–Nicolson time-stepping schemes only, although we expect it will be applicable more widely—both in the sense of wider classes of model problems (involving nonlinearities, for instance) and in the sense of other varieties of numerical scheme. We have further demonstrated how the technique applies in the case when the space mesh and time-step length vary between time steps, which presents the interesting conundrum of devising mesh refinement schemes that behave well when the mesh transfer error is accumulated in an $L^\infty(0,t)$ fashion.

Acknowledgements

The author would like to thank T. Pryer for many useful comments on the manuscript.

Funding

Engineering and Physical Sciences Research Council (EP/P000835/1).

References

Adams, R. A. & Fournier, J. J. F. (2003) *Sobolev Spaces, 2nd edn*. Pure and Applied Mathematics, vol. 140. Amsterdam: Elsevier/Academic Press, pp. xiv+305.

Ainsworth, M. & Oden, J. T. (2000) *A Posteriori Error Estimation in Finite Element Analysis*. Pure and Applied Mathematics. New York: Wiley-Interscience John Wiley & Sons, pp. xx+240.

Akrivis, G., Makridakis, C. & Nochetto, R. H. (2006) *A posteriori* error estimates for the Crank–Nicolson method for parabolic equations. *Math. Comp.*, **75**, 511–531.

Bangerth, W., Hartmann, R. & Kanschat, G. (2007) deal.II—A general-purpose object-oriented finite element library. *ACM Trans. Math. Software*, **33**, 24–27.

Bänsch, E., Karakatsani, F. & Makridakis, C. (2012) *A posteriori* error control for fully discrete Crank–Nicolson schemes. *SIAM J. Numer. Anal.*, **50**, 2845–2872.

Bänsch, E., Karakatsani, F. & Makridakis, C. (2013) The effect of mesh modification in time on the error control of fully discrete approximations for parabolic equations. *Appl. Numer. Math.*, **67**, 35–63.

Beirão da Veiga, L., Brezzi, F., Cangiani, A., Manzini, G., Marini, L. D. & Russo, A. (2013) Basic principles of virtual element methods. *Math. Models Methods Appl. Sci.*, **23**, 199–214.

Brenner, S. C. & Scott, L. R. (2008) *The Mathematical Theory of Finite Element Methods, 3rd edn*. Texts in Applied Mathematics, vol. 15. New York: Springer, pp. xviii+397.

Cangiani, A., Georgoulis, E. H., Pryer, T. & Sutton, O. J. (2017) *A posteriori* error estimates for the virtual element method. *Numer. Math.*, **137**, 857–893.

Chen, Z. & Feng, J. (2004) An adaptive finite element algorithm with reliable and efficient error control for linear parabolic problems. *Math. Comp.*, **73**, 1167–1193.

Clément, P. (1975) Approximation by finite element functions using local regularization. *Rev. Française Automat. Informat. Recherche Opérationnelle Sér.*, **9**, 77–84.

Eriksson, K. & Johnson, C. (1991) Adaptive finite element methods for parabolic problems I: a linear model problem. *SIAM J. Numer. Anal.*, **28**, 43–77.

Eriksson, K. & Johnson, C. (1995) Adaptive finite element methods for parabolic problems II: optimal error estimates in $L_\infty L_2$ and $L_\infty L_\infty$. *SIAM J. Numer. Anal.*, **32**, 706–740.

Ern, A., Smears, I. & Vohralík, M. (2017) Guaranteed, locally space-time efficient, and polynomial-degree robust *a posteriori* error estimates for high-order discretizations of parabolic problems. *SIAM J. Numer. Anal.*, **55**, 2811–2834.

Ern, A. & Vohralík, M. (2010) *A posteriori* error estimation based on potential and flux reconstruction for the heat equation. *SIAM J. Numer. Anal.*, **48**, 198–223.

Evans, L. C. (2010) *Partial Differential Equations, 2nd edn*. Graduate Studies in Mathematics, vol. 19. Providence, RI: American Mathematical Society, pp. xxii+749.

Gaspoz, F. D., Siebert, K., Kreuzer, C. & Ziegler, D. A. (2018) A convergent time-space adaptive dG(s) finite element method for parabolic problems motivated by equal error distribution. *IMA J. Numer. Anal.*, **3**, 181.

Georgoulis, E. H., Lakkis, O. & Wihler, T. P. (2017) *A posteriori* error bounds for fully-discrete hp-discontinuous Galerkin timestepping methods for parabolic problems, *Preprint.* arXiv:1708.05832.

Karakatsani, F. (2012) *A posteriori* error estimates for the fractional-step ϑ-scheme for linear parabolic equations. *IMA J. Numer. Anal.*, **32**, 141–162.

Kopteva, N. & Linss, T. (2013) Maximum norm *a posteriori* error estimation for parabolic problems using elliptic reconstructions. *SIAM J. Numer. Anal.*, **51**, 1494–1524.

KOPTEVA, N. & LINSS, T. (2017) Improved maximum-norm *a posteriori* error estimates for linear and semilinear parabolic equations. *Adv. Comput. Math.*, **43**, 999–1022.

LAKKIS, O. & MAKRIDAKIS, C. (2006) Elliptic reconstruction and *a posteriori* error estimates for fully discrete linear parabolic problems. *Math. Comp.*, **75**, 1627–1658.

LAKKIS, O., MAKRIDAKIS, C. & PRYER, T. (2015) A comparison of duality and energy *a posteriori* estimates for $L_\infty(0,T;L_2(\Omega))$ in parabolic problems. *Math. Comp.*, **84**, 1537–1569.

LIAO, X. & NOCHETTO, R. H. (2003) Local *a posteriori* error estimates and adaptive control of pollution effects. *Numer. Methods Partial Differential Equations*, **19**, 421–442.

LOZINSKI, A., PICASSO, M. & PRACHITTHAM, V. (2009) An anisotropic error estimator for the Crank–Nicolson method: application to a parabolic problem. *SIAM J. Sci. Comput.*, **31**, 2757–2783.

MAKRIDAKIS, C. (2007) Space and time reconstructions in *a posteriori* analysis of evolution problems. *ESAIM Proceedings. vol. 21 (2007) [Journées d'Analyse Fonctionnelle et Numérique en l'honneur de Michel Crouzeix]* (G. Caloz & M. Dauge eds). EDP Sciences: Les Ulis, pp. 31–44.

MAKRIDAKIS, C. & NOCHETTO, R. H. (2003) Elliptic reconstruction and *a posteriori* error estimates for parabolic problems. *SIAM J. Numer. Anal.*, **41**, 1585–1594.

PICASSO, M. (1998) Adaptive finite elements for a linear parabolic problem. *Comput. Methods Appl. Mech. Engrg.*, **167**, 223–237.

SEN GUPTA, J., SINHA, R. K., REDDY, G. M. M. & JAIN, J. (2016) *A posteriori* error analysis of two-step backward differentiation formula finite element approximation for parabolic interface problems. *J. Sci. Comput.*, **69**, 406–429.

SUTTON, O. J. (2017a) The virtual element method in 50 lines of MATLAB. *Numer. Algorithms*, **75**, 1141–1159.

SUTTON, O. J. (2017b) Virtual element methods. *Ph.D. Thesis*, University of Leicester, UK.

THOMÉE, V. (2006) *Galerkin Finite Element Methods for Parabolic Problems, 2nd edn*. Springer Series in Computational Mathematics, vol. 25. Berlin: Springer, pp. xii+370.

VERFÜRTH, R. (1998a) *A posteriori* error estimates for nonlinear problems. $L^r(0,T;L^\rho(\Omega))$-error estimates for finite element discretizations of parabolic equations. *Math. Comp.*, **67**, 1335–1360.

VERFÜRTH, R. (1998b) *A posteriori* error estimates for nonlinear problems: $L^r(0,T;W^{1,\rho}(\Omega))$-error estimates for finite element discretizations of parabolic equations. *Numer. Methods Partial Differential Equations*, **14**, 487–518.

VERFÜRTH, R. (2003) *A posteriori* error estimates for finite element discretizations of the heat equation. *Calcolo*, **40**, 195–212.

VERFÜRTH, R. (2013) *A Posteriori Error Estimation Techniques for Finite Element Methods*. Numerical Mathematics and Scientific Computation, Oxford: Oxford University Press, pp. xx+393.

WHEELER, M. F. (1973) *A priori* L_2 error estimates for Galerkin approximations to parabolic partial differential equations. *SIAM J. Numer. Anal.*, **10**, 723–759.

WIHLER, T. P. (2007) Weighted L^2-norm *a posteriori* error estimation of FEM in polygons. *Int. J. Numer. Anal. Model.*, **4**, 100–115.